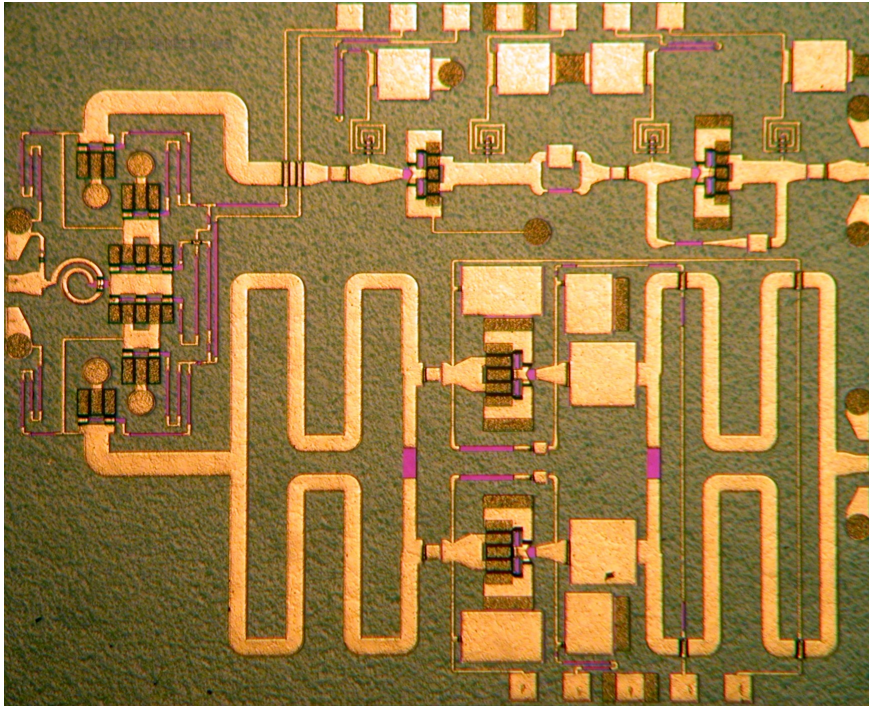




CHALMERS
UNIVERSITY OF TECHNOLOGY



Characterization of memory effects in GaN based HPAs for multi function sensors

Master's thesis in Wireless, Photonics and Space Engineering

Andreas Divinyi

MASTER'S THESIS 2020

Characterization of memory effects in GaN based HPAs for multi function sensors

Andreas Divinyi



CHALMERS
UNIVERSITY OF TECHNOLOGY

Department of Microtechnology and Nanoscience
Microwave Electronics Laboratory
CHALMERS UNIVERSITY OF TECHNOLOGY
Gothenburg, Sweden 2020

Characterization of memory effects in GaN based HPAs for multi function sensors
Andreas Divinyi

© Andreas Divinyi, 2020.

Manager: Ninva Shamoun, Saab AB
Supervisors: Mattias Thorsell, Saab AB, Peter Hammar, Saab AB

Examiner: Christian Fager, Department of Microtechnology and Nanoscience

Master's Thesis 2020
Department of Microtechnology and Nanoscience
Microwave Electronics Laboratory
Chalmers University of Technology
SE-412 96 Gothenburg
Telephone +46 31 772 1000

Cover: MMIC Transceiver

Typeset in L^AT_EX
Gothenburg, Sweden 2020

Characterization of memory effects in GaN based HPAs for multi function sensors
ANDREAS DIVINYI
Department of Microtechnology and Nanoscience
Chalmers University of Technology

Abstract

Truly multi-functional sensor systems are enabled through the recent development of wideband and multi channel digital back ends to control systems with several transmitter and receiver modules, in combination with the advancements in the development of these modules utilizing GaN MMIC based solutions. However, there is a considerable lack of insight into the problem of long term memory effects in broadband GaN MMIC power amplifiers required to enable the next generation of small and lightweight multi functional sensor systems. As such this thesis is focused on the impact of memory effects when changing between two waveforms representative of the different operating conditions applicable for a multi function system. Thus a suitable test bench is designed capable of providing arbitrary waveforms, switching between them and, record the results. The measurement data is modeled in terms of exponential time constants in order to quantify the impact on the behavior of a power amplifier caused by memory effects in terms of amplitude and time. The results indicate the presence of these memory effects in the amplifier operation after switching applications and decrease of influence from the previous waveform as time progress. Furthermore, investigating the effect of timing mismatch between the gate and RF pulsing showed a significant decrease in device performance.

Keywords: Characterization, GaN, MMIC, HPA, Memory effects, Multi functional sensors.

Acknowledgements

I would like to thank my manager at Saab Ninva Shamoun as well as Fredrik Ingvarson for the opportunity to perform my master's thesis at Saab. Special thanks to my supervisors Mattias Thorsell and Peter Hammar for their supervision, support, and willingness to discuss my work. I would also want to thank my examiner Christian Fager who always have been available to help and support in matters involving my thesis. Thanks to all the people at Saab who have taken their time to provide feedback and discuss my progress throughout the project. Especially Olle Axelsson and Henrik Voss for helping me get the amplifiers operational and provide technical assistance. I would also like to thank my opponent Isabel Tidekrans for her insightful comments about my thesis. Without all of your involvement and support this thesis would not have been possible.

Andreas Divinyi, Gothenburg, June 2020

Contents

| | |
|--|-------------|
| List of Figures | xi |
| List of Tables | xiii |
| 1 Introduction | 1 |
| 2 Multi functional sensors | 3 |
| 2.1 AESA | 3 |
| 2.2 Radar | 4 |
| 2.3 Electronic warfare | 5 |
| 2.4 Communication | 5 |
| 2.5 Multi function sensors | 6 |
| 3 GaN Technology | 7 |
| 3.1 GaN material properties | 7 |
| 3.2 The GaN HEMT | 8 |
| 3.3 MMIC | 9 |
| 4 Test-bench for multi functional sensors | 11 |
| 4.1 Requirements | 11 |
| 4.2 Measurement setup overview | 11 |
| 4.3 Waveform sequencing | 13 |
| 4.4 Bias control | 15 |
| 4.5 Recording output | 17 |
| 5 Modelling | 19 |
| 5.1 Modelling of results | 19 |
| 6 Measurement results | 21 |
| 6.1 Test case 1 | 21 |
| 6.2 Test case 2 | 31 |
| 6.3 Test case 3 | 39 |
| 7 Conclusion | 45 |
| 8 Future work | 47 |
| 9 Environmental and ethical aspects | 49 |

Bibliography

51

List of Figures

| | | |
|-----|---|----|
| 2.1 | A conceptual schematic over a radar system. | 4 |
| 2.2 | A basic transmitter consisting of waveform generation and amplification. | 4 |
| 3.1 | A general not to scale schematic over a typical GaN based HEMT and the different contacts and layers that comprise the device. | 9 |
| 4.1 | A conceptual circuit over the intended measurement setup | 12 |
| 4.2 | The measurement flow is a sequence of actions that consists of configuring and enabling the system before pulse generation and recording of system output. | 13 |
| 4.3 | A flowchart over the content of the sequence in the AWG. The sync marker is connected to the Oscilloscope and triggers the measurement. The advance command is being output by the measurement routine at a desired time. | 14 |
| 4.4 | Example of the gate pulsing and RF pulsing when the gate is enabled before, during and after the RF pulse | 16 |
| 5.1 | Example of measurement data along with fitting. Notice the highlight of the exponential curves used to model transients. | 20 |
| 6.1 | Illustration of the effect of saturation in a amplifier. Note that the illustration is not to scale. | 22 |
| 6.2 | Illustration of measurement scenario, not to scale and blue dots used to illustrate that there are 10 minutes between the measurements. The first waveform is high power and operated in non linear amplification regime while second waveform is comparatively low power in linear regime. | 23 |
| 6.3 | Non linear operating mode for two different compression points 1 and 5dB for two different version of a HPA. HPA A (left) and HPA B (right). | 25 |
| 6.4 | Linear operation mode for the initial pulses at the switch non linear and linear for three different compression points 1,3 and 5dB for two different version of a HPA. HPA A (left) and HPA B (right). | 26 |
| 6.5 | Linear operation mode reference measurement 10 min after switch for two different compression points 1 and 5dB for HPA A and B. | 29 |

| | | |
|------|--|----|
| 6.6 | The gate and RF pulse mismatch, note that RF pulse is applied before gate pulse, note that illustration is not to scale. | 32 |
| 6.7 | Non linear operation mode measurement for two compression points 1 and 5dB for HPA A (left) and HPA B (right). | 33 |
| 6.8 | Linear operation mode initial measurement , HPA A (left) and HPA B (right). | 35 |
| 6.9 | Linear operation mode reference measurement, 10 min after switch from non linear , HPA A (left) and HPA B (right). | 38 |
| 6.10 | Illustration of measurement scenario, not to scale. The non linear operating mode is pulsed and high power and is switched to linear operating mode and a long pulse illustrated by a 6ms trailing RF modulated pulse. | 40 |
| 6.11 | The measured switch between pulsed RF and CW with the measurement starting with the last pulse and then CW for two versions of an amplifier. The more recent version to the right and the older version to the left. The bottom half provides a zoomed in version to the above measurements. | 42 |
| 6.12 | The measured current during switch from pulsed to CW. Note that the below graphs are zoomed in around the waveform switch. | 43 |

List of Tables

| | | |
|------|--|----|
| 6.1 | Settings used to investigate the impact of compression. | 22 |
| 6.2 | The resulting parameters are from the model fitting to the non linear high power operation mode reference measurement for HPA A for three compression points | 24 |
| 6.3 | The resulting parameters are from the model fitting to the non linear high power operation mode reference measurement for HPA B for three compression points | 25 |
| 6.4 | The resulting parameters from the model fitting to the measurement data from HPA A for linear operating mode, initial pulses | 27 |
| 6.5 | The resulting parameters from the model fitting to the measurement data from HPA B for linear operating mode, initial pulses. | 27 |
| 6.6 | The resulting parameters from the model fitting to the measurement data from HPA A for linear operating mode, reference measurement. | 30 |
| 6.7 | The resulting parameters from the model fitting to the measurement data from HPA B for linear operating mode, reference measurement. | 30 |
| 6.8 | Settings used to investigate the impact of gate and RF pulsing time mismatch. | 31 |
| 6.9 | The resulting parameters are from the model fitting to the non linear high power operation mode reference measurement for HPA A, mismatched pulsing, for three compression points. | 34 |
| 6.10 | The resulting parameters are from the model fitting to the non linear high power operation mode reference measurement for HPA B, mismatched pulsing, for three compression points. | 34 |
| 6.11 | The resulting parameters from the model fitting to the measurement data from HPA A for linear operating mode, initial pulses for mismatched pulsing. | 36 |
| 6.12 | The resulting parameters from the model fitting to the measurement data from HPA A for linear operating mode, initial pulses for mismatched pulsing. | 36 |
| 6.13 | The resulting parameters from the model fitting to the measurement data from HPA A for linear operating mode, reference measurement, mismatched pulse case. | 37 |
| 6.14 | The resulting parameters from the model fitting to the measurement data from HPA B for linear operating mode, reference measurement. | 37 |
| 6.15 | Settings used in the pulsed to continuous wave measurement. | 39 |

1

Introduction

The demand for more sensors in everything from mobile phones, cars and drones drives the development of smaller, lighter, and more efficient sensor systems. There is also a demand for the capability to be able to do more with these sensors, preferably replacing several systems with one is a general trend [1] [2]. The case of airborne surveillance systems is perhaps one of the best examples where the demand for small, lightweight. and versatile systems is prominent due to the inherent limitations in confining multiple systems in an aircraft.

One relevant technology to implement and make use of multi function sensors is active electronically scanned arrays (AESA). This is a suitable technology for the implementation of a multi function sensor system. By consisting of a large number of antenna elements separately controlled through a digital back end enables greater freedom in using beamforming [2]. Thus the system can function as if it was several antennas pointed in different directions. These beams can then be utilized for different functions or in support of the same use case. This could include but not be limited to an AESA that incorporates a radar system, communication, and electronic warfare [2]. Due to the possible use cases for these systems, the demand for sensor reliability and performance is highly prioritized. Failure to achieve this might degrade the quality of transmitted or received information or even render it useless. The implications of this in a military or civilian implementation could potentially put lives at risk as well as endanger valuable property.

The intended functionality of the AESA poses several demands on the construction of the front end regarding both the choice of technology and material. For instance, it needs to comply with the demand for small size and weight considerations. While still provide high amplification for the transmitter and receiver sensitivity for the applications that requires this. The system is also required to maintain a high degree of power efficiency in order to not require excessive cooling which also require energy. Thus depending on intended use smart use of multi function systems could also reduce power consumption with possible environmental benefits as a result. For these reasons, the best suited alternative is a gallium nitride (GaN) based solution made with monolithic microwave integrated circuit (MMIC) for use in the front end in an AESA system [3]

Furthermore, GaN is a wide band gap semiconductor which has proven to be the most capable of operating at frequencies up to W-band (75 GHz-110 GHz) [4]. Used in high electron mobility transistors (HEMT) it has proven to be able to handle large

amounts of power and operating more efficiently than competing technologies. The advent of using GaN based solution has revolutionized the semiconductor industry focused on high power applications. There is however a multitude of decisions regarding growth, design and manufacturing, and their impact to take into consideration. For example how buffer doping cause time dependant electron trapping in the amplifier resulting in a temporary decrease in gain [5].

Therefore as multi function sensors are being implemented there is a need to more thoroughly characterize and understand memory effects. Especially as the operation of an AESA requires reliable switching between applications or waveforms. The intention is that the system immediately should be able to rely on the front end, such as power amplifiers, to remain linear regardless of a previous application. However, since the presence of memory effects has been proven it is thus known that there are non linear effects. Furthermore, the cause of these effects in GaN high power amplifiers is known and has been extensively studied in terms of pulse to pulse instability [6] [7]. Along with studies of the non linearities such as hot electron trapping in GaN devices [8]. Similarly, there has been research into the field of modeling and compensating of transients in GaN amplifier [9]. However these models aim to compensate for transients present during thermal equilibrium of pulses in GaN power amplifiers but do not take memory effects from the previous signal into consideration.

This illustrates a gap in the understanding of the initial impact of a waveform for the initial pulses. Previous research has not characterized the present memory effects in terms of the previous waveform that could have caused memory effects when initiating a waveform or signal. Therefore the impact of the memory effects is not known or how it varies depending on the properties of the waveforms considered. The thesis contributes with how to construct an appropriate test bench capable of characterizing the impact of switching between different waveforms. By doing this for the initial pulses and comparing it to steady state cases it is possible to estimate the impact of memory effects and quantify transients.

2

Multi functional sensors

There are instances where a platform, such as an aircraft, require the use of several sensors systems for a range of applications such as radar, communications system and depending on intended use also systems for electronic warfare. Providing separate sensors for all these systems however, represents not only a cost but also requires space and contributes to weight. Therefore, there are incentives to more efficiently use the available sensors. This is also seen in the trend to decrease sensor system complexity and reduce the amount of hardware necessary and replace several other systems with one. However, these systems are required to retain the previous functionality and also to improve performance and reliability.

2.1 AESA

Active electronically scanned array (AESA) is an implementation of a multi function system and is used for platforms including naval and airborne systems. To realize a multi functional AESA requires two parts, a digital back end, and a high performing front end to enable multi function applications [10]. The front end is comprised of an arbitrary amount of transmitter/receiver modules that can be subdivided and configured with beam forming and thus acting like separate antennas by applying a phase shift in the transmitted or received signal [1]. Separate beams are advantageous since the system can be made highly flexible and versatile by assigning different applications to different beams. This also enables reconfiguring the system and switching between applications due to the high degree of freedom in controlling the transmitter/receiver by electronically redirection the antenna beam. Combined these options enable the AESA to support and successfully operate a wide range of applications such as radar, communication, and electronic warfare [1].

2.2 Radar

Radar is an acronym and stands for radio detection and ranging, it is used for detecting range and velocity of objects from a distance and have a plethora of both military and civilian uses. The main principle is to send out a well defined electromagnetic signal and measure the echo. The time for the signal to travel back and forth gives information on the distance to a detected target [11] as illustrated in figure 2.1. Furthermore, doppler shifts in frequency caused by the object provide information on speed and direction.

To illustrate the most basic functionalities of a radar system as seen in figure 2.1 consists of a transmitter to send out the radar pulse and a receiver to receive the pulse. The transmitter which contains the focus of this thesis, the high power amplifier (HPA). The operation of a transmitter as seen in figure 2.2 typically includes the input of the desired signal from a waveform generator [11]. There are several choices for radar signals as both continuous wave (CW) and pulses can be utilized and they can be chirped or not. Before the signal is being sent out using the antenna the signal is required to be amplified. Ideally, to avoid distortion the amplification is simply the linear gain independent of the previous signal. Therefore the amplification step is critical for the radar to avoid distortions and increase performance [10].

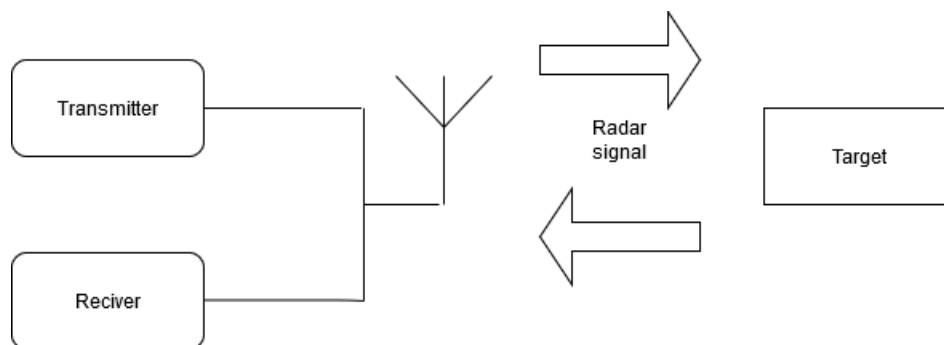


Figure 2.1: A conceptual schematic over a radar system.

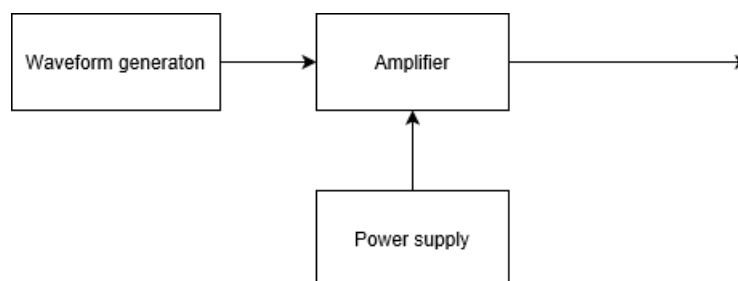


Figure 2.2: A basic transmitter consisting of waveform generation and amplification.

2.3 Electronic warfare

Electronic warfare can be divided into two categories, electronic support (ES) and electronic attack (EA). ES systems are mainly used for passively detecting signals from example enemy radars and provide the functionality to characterize and even locate the source of these signals. As it is a passive system does not require a transmitter but in order to be able to detect potentially broadband radar signal the ES on average needs a significant bandwidth [1].

However, the EA heavily relies on transmitters as it is intended for impacting the function of target systems. Utilizing different sorts of jamming technologies as an important feature for this system is the ability to output enough power to reduce the performance of an enemy sensor system. This is mostly done by simply having a signal that distorts or raises the noise floor of the signal the enemy system is intending to record. Therefore a functioning EA relies on the system being able to identify and provide a jamming signal on the frequency band utilized by the enemy. EA can also be used to provide false information to enemy systems by having ES analyzing an enemy radar signal and then having EA output an altered radar signal containing a false signal concerning location [1]. However, to enable such functionality requires that the amplifier is linear so as not to affect the false radar echo. This increases the difficulty of eliminating a radar system and thus reducing the risk of operating the system.

2.4 Communication

Use of communication could for a mobile or stationary radar system include communicating with other mobile platforms such as airborne systems (aircraft or drones), transfer of sensor data to a control center, or any other need for data transfer. The main requirements to do so is to have a sufficient signal power in order to establish a signal to noise ratio (SNR) to discern the signal from noise. Noise usually becomes an issue when the signal is attenuated by propagation or other effects [1]. There are other design considerations such if the data intended to be transmitted or received is time dependent. Then the bandwidth of the communication system needs to be large enough to allow a sufficient data rate [1]. This in turn could introduce the need to change to higher frequencies which in turn increases the demand for more power due to higher attenuation [1].

2.5 Multi function sensors

AESA enables a platform to utilize multi function operations and the reduced complexity that it provides [10], while at the same time taking advantage of improved reliability and functionality. In a military context, the multi function sensors could be implemented in systems that provide radar functionality such as detection and ranging. Furthermore, simultaneously be equipped to function as jamming and communication systems. This has potential especially for airborne platforms [10] because these are already equipped with a large number of systems making the inclusion of more sensors unfeasible as the demand for more EA and communication rise. By taking advantage of multi function systems reduce the amount of equipment needed. This in turn enables an airborne system even more lightweight which is of advantageous for possible drone based systems. Furthermore, the software needed to operate these intended systems with multi function sensors other requirements include support for multiple waveforms and concerning hardware reliable RF sources [10].

3

GaN Technology

Using gallium nitride based solutions in multi function sensor front ends has proven to be the best alternative to reduce the size and enable versatile use. This is possible due to several reasons such as intrinsic material properties and its usefulness in designing HEMT based amplifiers with MMIC and the advantages in performance and fabrication.

3.1 GaN material properties

The GaN semiconductor has proven to be the best suited material for use in high power RF applications due to several intrinsic properties such as a wide band gap and high mobility [12]. A feature of the wide band gap is a higher breakdown voltage which enables it to be used directly in high power components [12]. Furthermore, a low electron transit time in the crystal gives rise to a high cutoff frequency enabling the material being used for high frequency applications [4]. However, the product of cutoff frequency and breakdown voltage is called the Johnsson's limit and is used as a figure of merit to indicate the trade off between breakdown voltage and cut-off frequency. This is a material dependent figure and increasing the breakdown decreases the cutoff frequency and thus to enable both a high frequency and high power application this value needs to be sufficiently high in order to operate at high power and high frequency [4]. For example, if normalized with the value for Si, the Johnsson's limit of GaN is 27.5 while a material such as GaAs has a value of 2.7 [13].

The process of growing GaN crystals has been successful with both metal organic chemical vapor deposition (MOCVD) and molecular beam epitaxy (MBE). Both of these techniques are capable of growing a thin layer of GaN another semiconductor materials. This is what enables the design of components out of this material [12]. However, in terms of manufacturing the MOCVD process has proven more suitable as it is faster and cheaper compared to MBE. Unfortunately using MOCVD introduces impurities into the GaN crystal which causes to become more conductive introducing leakage currents. To decrease these leakage currents it is a common design choice to dope the material with Fe atoms. This, in turn introduces another unwanted effect by causing trap states in the band gap of the device. [14] [5].

3.2 The GaN HEMT

Creating a hetero junction by placing AlGa_N on top of Ga_N can be used for fabricating high electron mobility transistor (HEMT) which is regarded as a desirable component for use in high frequency and high power system. This due to it allowing high current densities while achieving a low channel resistance thus reducing the amount of heat. This is the result of the creation of a two dimensional electron gas (2DEG) in the interface between AlGa_N and Ga_N [15]. The 2DEG is located in the Ga_N portion between the buffer and the AlGa_N layer as illustrated in figure 3.1. Depending on the design the Ga_N HEMT has a high amount of electrons in the 2DEG even with no applied gate voltage making the Ga_N HEMT an always on device.

The HEMT consists of several layers as seen in figure 3.1 and the device can be constructed on a substrate consisting of SiC. On top of the substrate is the AlN nucleation layer which decreases the lattice mismatch between SiC and Ga_N making it possible to grow Ga_N on top of the AlN layer [15]. The mismatch is caused by differences in crystal structure between the two materials causing a strain in the material. If the mismatch is too large the crystal lattice will not be able to align with each other as a continuous crystal structure. This is the case of SiC and Ga_N introducing the need for the AlN nucleation layer. There are however other substrate solutions that mitigate this effect but SiC is at the moment the most common alternative for high performance components [15]. However, the Ga_N layer is even though the presence of the nucleation layer of rather poor quality. To improve the Ga_N quality a thicker layer is required to reduce the defect density in the crystal. Unfortunately, the MOCVD process introduces impurities during fabrication and makes the Ga_N more conducting. To counteract this the layer is Fe doped to make it more restive in order to decrease leakage currents.

The AlGa_N/Ga_N interface creates a heterojunction and due to differences in polarization in the material a two dimensional electron gas is formed the 2DEG. This creates a high density of electrons which can be used to conduct current in the device by applying a voltage over Drain and Source in figure 3.1. These contacts are ohmic since they are intended for conducting current through the device in contrast to the gate that is metal placed directly on the AlGa_N creating a Schottky barrier. The gate is then used to control the amount of carriers in the 2DEG, and by applying a negative voltage on the gate it is possible to reduce the amount of charge carriers and thus decrease the current [5].

The trap electron states introduced by Fe doping during operation creates a charge in the buffer and acts as a backgate by decreasing the amount of available carriers and thus decreases the current and gain. The traps are typically filled when a high electric field is applied such as when the device is being used for high power applications [14]. The electron states are therefore relevant in the context of memory effects especially in the case of switching between high and low power applications where the higher power levels have been shown to correspond to a higher degree of

distortion [14].

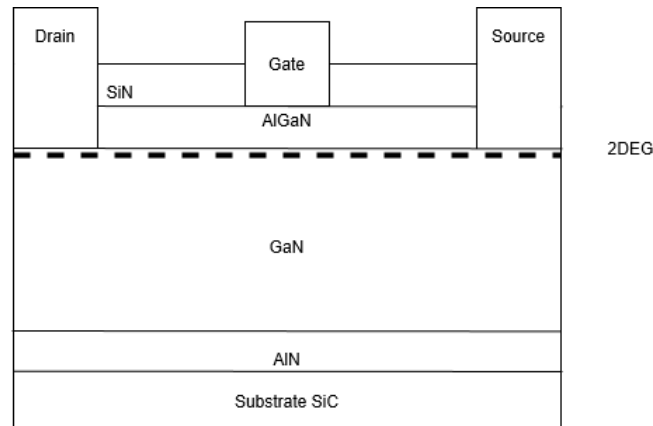


Figure 3.1: A general not to scale schematic over a typical GaN based HEMT and the different contacts and layers that comprise the device.

3.3 MMIC

To use GaN HEMTs in a multi function system the Monolithic microwave integrated circuit (MMIC) technology has been identified as a suitable technique for use in designing front ends in multi function systems such as AESA [3]. By utilizing MMIC it is possible to construct entire components such as an amplifier directly on a chip [16]. The concept is to integrate and fabricate both active and passive components on the same wafer. Having the entire device integrated on the wafer has proven to have several advantages including smaller size and fabrication of larger amounts of components [12].

The great advantage of using just GaN based MMIC solutions is that GaN is suitable not only for HPA but also for Low noise amplifiers (LNA). The implication of this is that not only the transmitter but also the receiver can be manufactured on the same chip [16]. Thus it is possible to construct transmitter/receiver modules meaning that in practice most of the transmitter/receiver chain as seen in figure 2.1 can be realized on a single chip [16]. This is ideal for AESA systems since it allows for the fabrication of large amounts of these modules at a lower price. To balance performance and economical viability the choice and quality on the wafer or the substrate to allow for ease in manufacturing but also thermal properties. Presently there are several companies that develop or supply substrates, apply epi layer, or perform MMIC for example II-VI supplies SiC substrate or UMS MMIC foundry. The interest in GaN in MMIC is large and the continual improvement in both manufacturing processes and material is of importance to further develop the technology used in the AESA front ends marking the significance of these solutions.

4

Test-bench for multi functional sensors

Evaluating the impact of memory effects at the switching instance for two waveforms poses several challenges both in terms of providing a controlled switching between waveforms as well as time the recording of data. To achieve this requires a measurement routine to enable a higher degree of control by automating the different tasks needed to perform the measurements.

4.1 Requirements

The main feature is to enable investigation of the impact memory effect due to previous waveforms. Thus the following criteria were deemed necessary to enable the output, controlled change of waveforms, and to record the effects.

- All the instruments needs to support remote control.
- Providing pulses
 - Be able to output modulated RF-pulses with carrier frequencies in the GHz.
 - Generation and upload of arbitrary waveforms.
- Well defined and controlled switching between waveforms marked by trigger signals.
- System must be able to operate with a signal amplitude range of minimum 10dB.
- Record system output signal with sufficient sampling rate to avoid aliasing.
- Reliable HPA biasing.
- Well defined and flexible gate pulsing
- Securely bias the device in order reduce the risk of damaging it.

4.2 Measurement setup overview

To illustrate the main function, a general chart of the test-bench in figure 4.1, followed by a more descriptive explanation of the different parts. For processing results as well as controlling the measurements the programming language Python version 3.7.2 was used, there are other alternatives but it was deemed an open source and platform independent programming language was desirable.

The central component in the test bench was the Arbitrary waveform generator (AWG). In the setup, an M8190A AWG was equipped with a 8 Gsample sampling

rate and a 12 bit resolution [17] which allowed for RF modulated pulses. An advantage with the choice of AWG is that it has two independent channels. Channel 1 is used for RF pulses while channel 2 was used for gate pulsing and with the sync marker were used to trigger other instruments in the setup. The measurement also began with generating and uploading the waveform as can be seen in figure 4.2. However, the AWG has a limited output power and for this reason, a lab amplifier BZ3-0218-552227-202525 which has a well defined and stable gain is used in order to achieve sufficient input power levels into the HPA. To bias the device, two power supply units are used and to control the gate bias of the HPA a TI control circuit were used.

The output from the HPA was then attenuated to safe power levels to be recorded by the oscilloscope, an RTO1044. To avoid aliasing it is important that the Nyquist criteria is fulfilled which are taken into consideration with the RTO1044 sampling rate of 10 Gsample/s. Using one channel to record the HPA output signal and another channel for the current measurement of the drain current using a current probe. A sync marker from the AWG at the switching moment was used to trigger the oscilloscope to begin recording the initial pulses. In order to phase lock the AWG and the oscilloscope, a 10MHz reference output from the oscilloscope is used. To further illustrate this, the main actions performed during the measurement is visualized in figure 4.2.

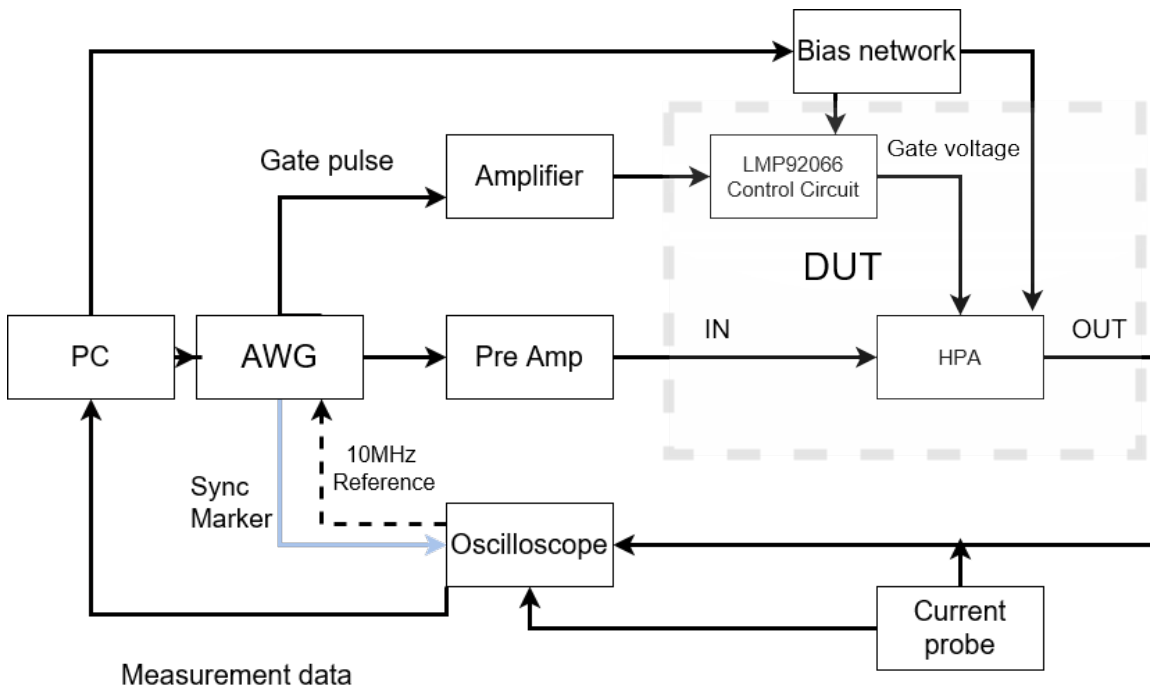


Figure 4.1: A conceptual circuit over the intended measurement setup

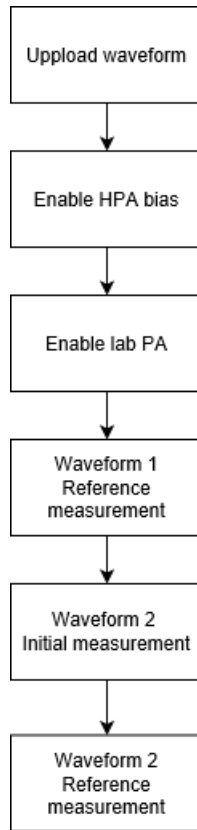


Figure 4.2: The measurement flow is a sequence of actions that consists of configuring and enabling the system before pulse generation and recording of system output.

4.3 Waveform sequencing

The essential part of the thesis is the study of the behavior of the resulting output from the HPA immediately after a change of waveform and wait for steady state before performing another measurement. This in order to compare the different measurements. Therefore it is desirable to be able to change most properties of waveform 2, for example, different frequency and amplitude. This requires a system capable of providing a consistent waveform 1 and then changing to waveform 2 while being able to register this change in order to reliably record the first pulse of waveform 2. This is done using the M8190A arbitrary waveform generator and its sequencing capabilities. By creating the desired waveforms first in python and upload these along with the desired configurations into the AWGs memory. Thereafter it is as illustrated in figure 4.3 possible to program the appropriate function of the AWG.

As it is the memory effects on waveform 2 that is of most interest, the measurement should begin with the switch from waveform 1 to 2. This is accomplished by configuring the setup to wait for a trigger before recording output. This method is valid for most waveforms and scenarios but as the thesis will focus on pulsed RF the waveform generated will reflect that. Thus the waveform 1 and 2 will be variations of pulsed RF, a pulse with a carrier frequency imposed upon it.

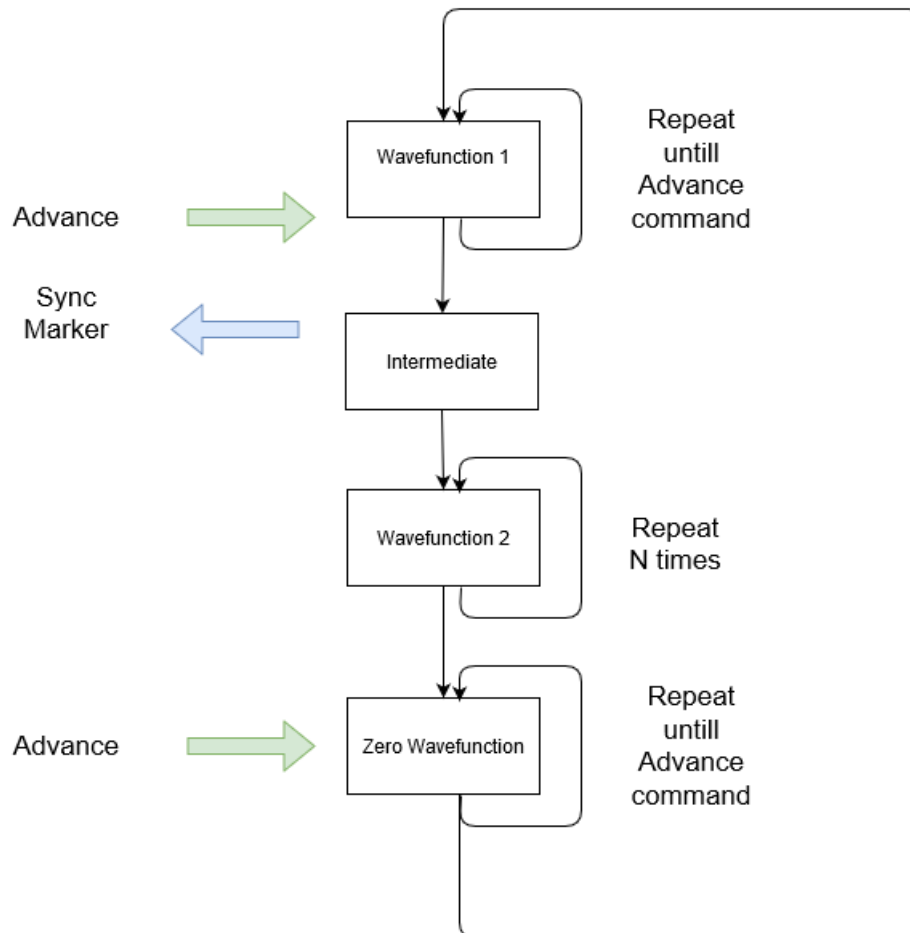


Figure 4.3: A flowchart over the content of the sequence in the AWG. The sync marker is connected to the Oscilloscope and triggers the measurement. The advance command is being output by the measurement routine at a desired time.

4.4 Bias control

The bias voltage was supplied by two power supplies a Hameg HMP4040 and a TTI CPX400DP. The TTI was used for biasing the lab PA located between the AWG and the HPA with 15 V and 580 mA needed for operation [18]. It also provided the drain voltage for the HPA. The Hameg was used to bias the control circuit with the necessary voltages 5 V, -5 V, and 3.3 V. Due to the operation of GaN PAs it is important that the device is properly biased as it is a normally on device [19]. For this reason, a safety mechanism was implemented in the measurement code that checks the output status of the Hameg before enabling the drain voltage when starting up the test bench. Similar at the end of a measurement the biasing from the Hameg is not turned off until it has been verified that the drain voltage is off.

To provide gate pulsing the AWG has two independent channels and the second is used to pulse the control circuit of the HPA which consists of a Texas instruments LMP92066 DAC that controls the gate bias. This enables the device to be biased with a sufficient negative voltage to ensure that the GaN HPA that is normally always on is in fact off unless the control circuit is pulsed. This was done by defining a matching sequence to the one used for RF pulses but without the carrier.

By pulsing the gate slightly before and slightly longer than the pulsed RF itself the gate was open when needed but is not left always open this is seen in figure 4.4. However, the method for controlling the gate pulsing enables freedom in controlling the timing between gate and RF pulses due to the AWG versatility. Thus figure 4.4 is only a possible configuration as the gate pulse can be configured to be enabled at a specified time before the RF pulse. This also enables the study of enabling the RF before gate investigating the effects of timing between RF and gate pulsing.

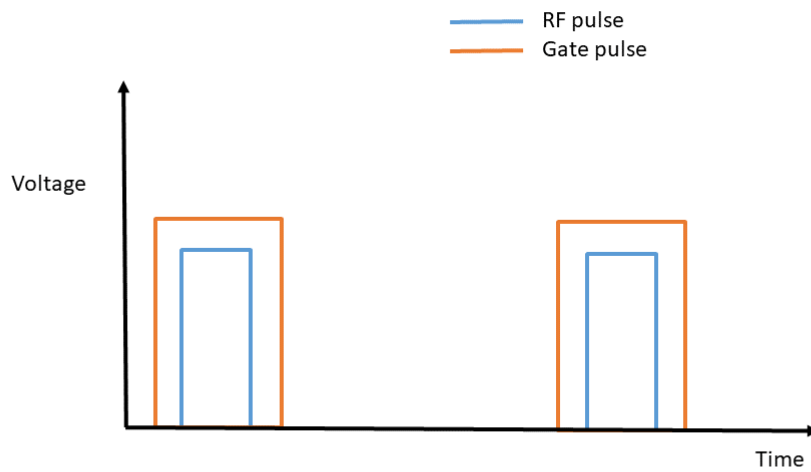


Figure 4.4: Example of the gate pulsing and RF pulsing when the gate is enabled before, during and after the RF pulse

4.5 Recording output

The previous sections have explained how the test bench is constructed in order to enable the generation of waveforms and function of the HPA. However, in order to be able to analyze the resulting signal, there is the need for recording and saving the information. To facilitate this the oscilloscope RTO1044 was chosen based on the sampling frequency of 10 GSample/s, the bandwidth of 4 GHz and possibility of programming [20]. The RTO1044 is able to record 100 MSample which with the sampling frequency corresponds to 10ms of pulses for the used sampling frequency. Important to note is the implication of wide bandwidth for measuring enables the study of the range of applications which can be of interest in the case of multi function sensors. Unfortunately, it also results in higher levels of thermal noise. This becomes an issue as the oscilloscope needs to operate over a wide amplitude range which is utilised in order to measure scenarios where the difference in amplitude between waveform 1 and 2 might be over 10dB depending on measurement scenario. The issue of SNR becomes more relevant for the lower amplitude and it is important to be aware of the trade off that arises from using a wide range of amplitude and SNR for the lower amplitude cases.

There are two different sorts of measurements that are to be carried out by the RTO1044 that requires changes in settings. The first being the reference measurements conducted before and several minutes after the change of waveform. In this measurement, the need to know exactly the pulse number of the reference pulses is not as important as having the waveform in a steady state. Thus the recording of these reference pulses can simply be started by triggering on the pulses themselves. The reference pulses of waveform 1 are recorded after 10 minutes of operation followed by reference measurement followed by waveform 2 that is recorded 10 minutes after the change from waveform 1 to 2.

Recording the initial pulses after the waveform changes however, requires more precision and is therefore started using a trigger signal which is sent out 2.5 μ s before the change of waveform in order to start the measurement. The start of the reference measurements however does not require more timing than that provided by a timer in measurement code. This measurement can thus be triggered by the positive slope of the signal itself and thereafter record 10 ms of data. After measurement, the data is downloaded from the oscilloscope onto the PC to be processed.

5

Modelling

In order to investigate the impact of memory effects, it is desirable to compare the reference measurements conducted before and after with the initial pulses immediately following the change of waveform. To enable such a comparison the measurement data were used to fit a model deemed representative of the behavior of the HPAs based on previous research [8].

5.1 Modelling of results

Modeling the data from the measurements were done in order to extract data with the intention to quantify differences in the behavior in HPA due to memory effects or change of transients due to waveform choice. To enable this the HPA behavior is described as a sum of exponential terms [8]. For this thesis, the model used was based on three exponentials.

$$f(t) = C_1 e^{\frac{-t}{\tau_1}} + (1 - C_2 e^{\frac{-t}{\tau_2}}) + C_3 e^{\frac{-t}{\tau_3}} \quad (5.1)$$

In order to facilitate the model fitting, some manual adjustments were necessary to take the variation in power level between waveform 1, intended to be of higher power level, and waveform 2 intended to be of lower power level into consideration. The adjustments consisted of applying an offset that would correspond to the offset in power level between the two in order to enable a comparison of the fitted parameters. Furthermore to achieve the optimal model fitting the least square algorithm for nonlinear functions implemented in MATLABs `lsqnonlin` function was used.

As seen in the figure 5.1 different exponentials were used to model the HPA output. The first term describes the initial fast high amplitude transient in the first microseconds of the pulse. Followed by an upwards trend and a relatively slower low amplitude transient. To facilitate a fit as shown in the figure 5.1 an estimation based on the equation (5.1) followed by a numeric optimization using a nonlinear least-squares data fitting to find the parameters corresponding to the best fit.

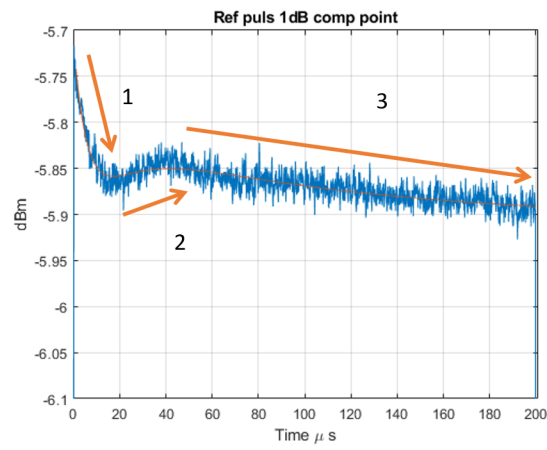


Figure 5.1: Example of measurement data along with fitting. Notice the highlight of the exponential curves used to model transients.

6

Measurement results

The characterization of a device is an important step in verifying intended performance, models and provide information for potential further development. For this reason, the previously described test-bench in chapter 4 is used to characterize two HPAs with respect to memory effects. The amplifiers are provided by Saab and are of the same model but two different versions, one older and one more recent version hereafter referred to as HPA A and HPA B. The reason for including two amplifiers is that it provides more statistics to base conclusions on. They should have comparable performance and only minor differences should be present. Therefore if large differences are observed, this would be relevant information for further development.

In order to characterize the amplifiers, three test cases have been chosen that represent different transitions between waveforms that would be representative for intended use cases. The first test evaluates the impact of operating the amplifiers in the nonlinear gain region before switching to a linear mode of operation for pulsed RF. The second test is similar to the first but introduces flexibility in setting the timing mismatch between gate pulse and RF pulse. The third scenario evaluates how the nonlinear drive level impacts a linear mode of operation for a continuous wave (CW) stimuli rather than a pulsed operating mode.

6.1 Test case 1

Ideally, an amplifier should have a linear behavior with a gain that is constant regardless of input power as seen in the ideal case in figure 6.1. However, in reality, the amplifier is only able to provide a constant gain up to a certain point thereafter the gain starts to saturate, the amplifier is starting to experience compression as illustrated by the dashed line in figure 6.1. In order to indicate the amount of compression, it is possible to use for example the 1dB compression point which indicates the point where the gain is 1dB below the ideal level illustrated with the red arrows. The first test case is to investigate the impact of operating the HPAs in different nonlinear regimes corresponding to 1 and 5dB compression points and switching to an input drive power level in the linear regime. The settings for the measurements below are described in table 6.1 and include the pulse repetition interval (PRI), duty cycle, and the gate pulse is applied $2.5 \mu s$ before RF pulse. The delay between the gate and RF pulse is to make sure that the gate is opened before the RF is applied, which has been verified using an oscilloscope.

The reason for this measurement case is to determine the impact of memory effects on the initial pulses for linear operation mode due to the higher drive input power in a previous non linear operation mode. The scenario is illustrated in figure 6.2 and includes the three separate measurements that are performed. First after achieving steady state and conduct a reference measurement of the non linear operation mode in thermal equilibrium. The second is a measurement in the moment of switching between non linear and linear. The third is a reference measurement of the linear mode in thermal equilibrium. By performing the two reference measurements it is possible to compare the initial pulses in linear operation mode and conclude the impact of memory effects since the reference measurements should be stable while the initial pulses could be impaired due to memory effects. In the case of no memory effects, the initial pulses should be the same as the non linear reference measurement. In order to reduce the impact of noise the displayed graphs will be the average of 5 pulses.

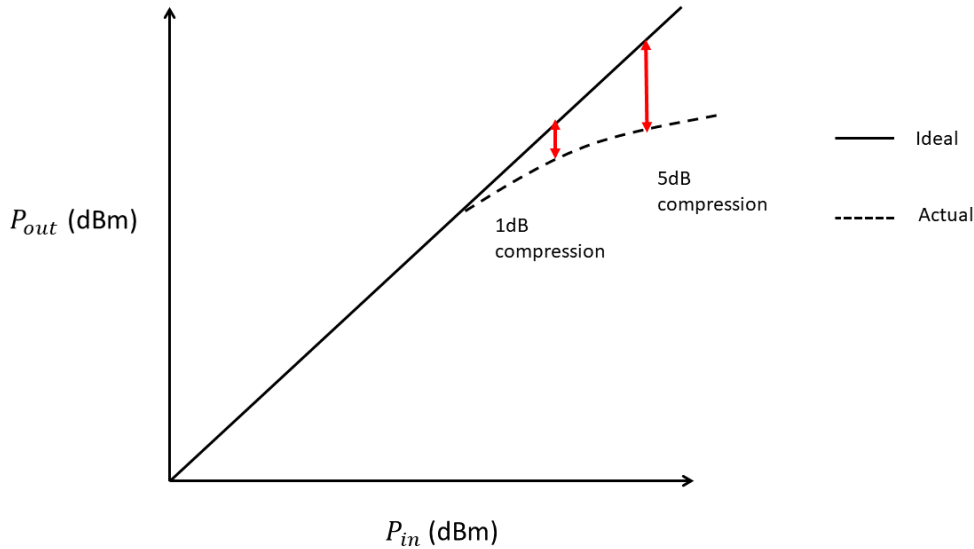


Figure 6.1: Illustration of the effect of saturation in an amplifier. Note that the illustration is not to scale.

Table 6.1: Settings used to investigate the impact of compression.

| Operation mode | PRI (ms) | Duty cycle (%) |
|----------------|----------|----------------|
| Non linear | 2 | 10 |
| Lineear | 2 | 10 |

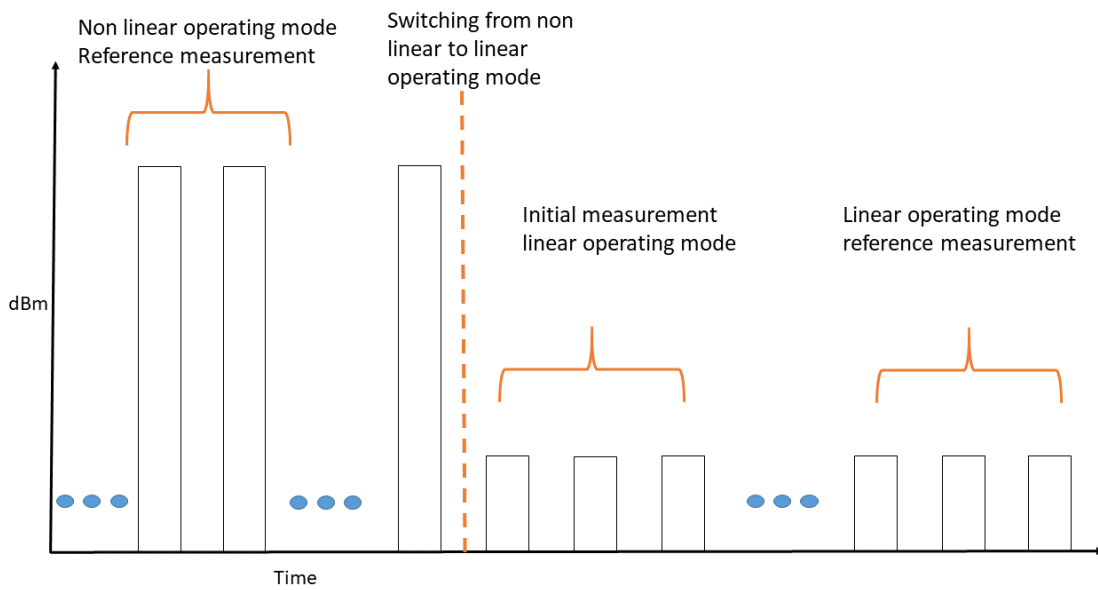


Figure 6.2: Illustration of measurement scenario, not to scale and blue dots used to illustrate that there are 10 minutes between the measurements. The first waveform is high power and operated in non linear amplification regime while second waveform is comparatively low power in linear regime.

The results from the non linear operating mode reference measurement are seen in figure 6.3 and illustrate the average of five pulses. Thus it can be seen that the initial transient is a fast, decreasing transient. This initial transient is prominent for the first $20\mu s$ of the pulse. After the initial decreasing transient an increasing transient starts and is dominant for another $20\mu s$ and is followed by a slower decreasing transient for the remainder of the pulse.

There are some differences between the different input drive levels as can be seen that the initial transient has a higher amplitude for the 5dB compression compared to 1dB. Furthermore, the two versions of the amplifier coincide quite well with some exceptions such as the HPA B seem to experience a more prominent second transient. The third transient for HPA B also has a higher amplitude resulting in a larger decrease in power during the later part of the pulse

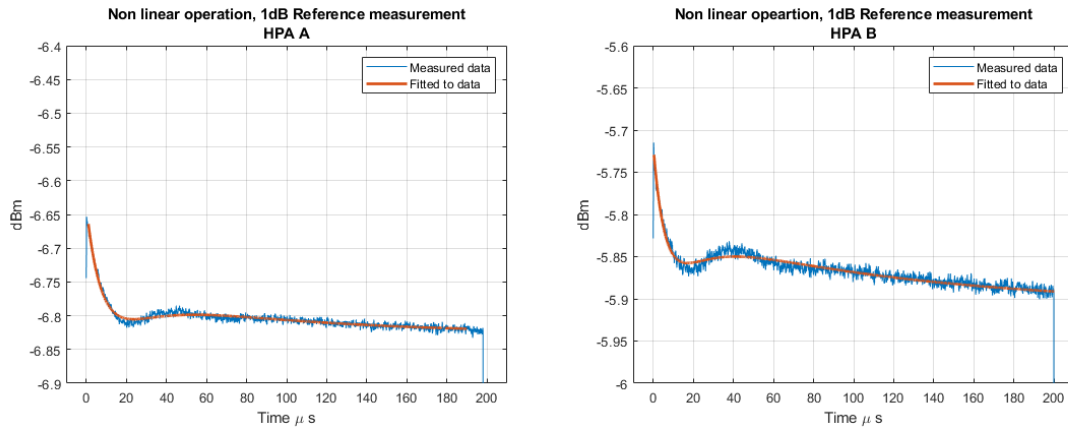
The response can be modeled by exponential transients as mentioned in chapter 5 with the index indicating which of the three transients the parameter is representing. As such the models for the different test cases are plotted in the respective graph and follow the same trend as the measurement data. As such the model parameters for the fit are included in table 6.2 for HPA A and table 6.3 for HPA B. The parameter C_1 is larger than C_2 which in turn is larger than C_3 which corresponds with the observed behavior in the graphs. Similarly, the time constants τ_1 , τ_2 , and τ_3 corresponds to increasingly slower transient which also coincides with the observed trend in the graphs. The C_1 and C_2 parameters also increase in terms of increasing non linear drive levels. The fitted model parameters for the two amplifiers agree with each other with the main difference being the 3dB compression point measurement for the HPA B which differs from the corresponding measurements for HPA A with a factor 2 which could indicate a small difference between the amplifier.

Table 6.2: The resulting parameters are from the model fitting to the non linear high power operation mode reference measurement for HPA A for three compression points

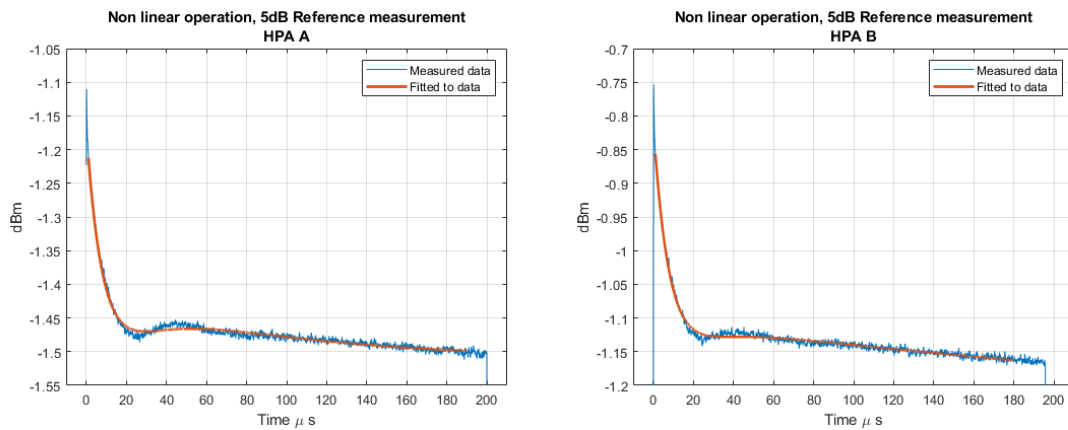
| Non linear operation reference measurement, HPA A | | | | | | |
|---|-------|-----------------|-------|-----------------|-------|-----------------|
| Parameters | C_1 | $\tau_1(\mu s)$ | C_2 | $\tau_2(\mu s)$ | C_3 | $\tau_3(\mu s)$ |
| 1dB | 0.291 | 8.083 | 0.175 | 18.58 | 0.073 | 77.02 |
| 3dB | 0.422 | 8.264 | 0.205 | 20.86 | 0.076 | 88.74 |
| 5dB | 0.522 | 9.051 | 0.290 | 18.08 | 0.119 | 83.93 |

Table 6.3: The resulting parameters are from the model fitting to the non linear high power operation mode reference measurement for HPA B for three compression points

| Non linear operation reference measurement, HPA B | | | | | | |
|---|-------|-----------------|-------|-----------------|-------|-----------------|
| Parameters | C_1 | $\tau_1(\mu s)$ | C_2 | $\tau_2(\mu s)$ | C_3 | $\tau_3(\mu s)$ |
| 1dB | 0.288 | 6.665 | 0.193 | 13.32 | 0.130 | 113.8 |
| 3dB | 0.450 | 9.066 | 0.260 | 15.17 | 0.124 | 370.0 |
| 5dB | 0.484 | 7.402 | 0.284 | 11.48 | 0.117 | 133.4 |



(a)



(b)

Figure 6.3: Non linear operating mode for two different compression points 1 and 5dB for two different version of a HPA. HPA A (left) and HPA B (right).

6. Measurement results

The initial pulses illustrated in figure 6.4 are measured at the switching between non linear operating mode and linear. Comparing this measurement of initial pulses for figure 6.4 with the previous non linear operating mode in figure 6.3 shows some differences. The first but also the second transient is not as prominent but follow the same trend of the first, second, and third transient. The previously observed difference between HPA A and HPA B with a higher decrease of gain towards the end of the pulse is present also for the linear operating mode.

Furthermore, the fitted model with the extracted parameters displayed in table 6.4 and table 6.5 for HPA A and B respectively. The different transient are comparable to that of the reference measurement for non linear operating mode in tables 6.2 and 6.3 in terms of how the different parameters compare in magnitude to each other. $C_1 > C_2 > C_3$ and $\tau_1 < \tau_2 < \tau_3$ for both operating mode. While simultaneously displaying a similar increase in C_1 and C_2 as the input drive power levels increase.

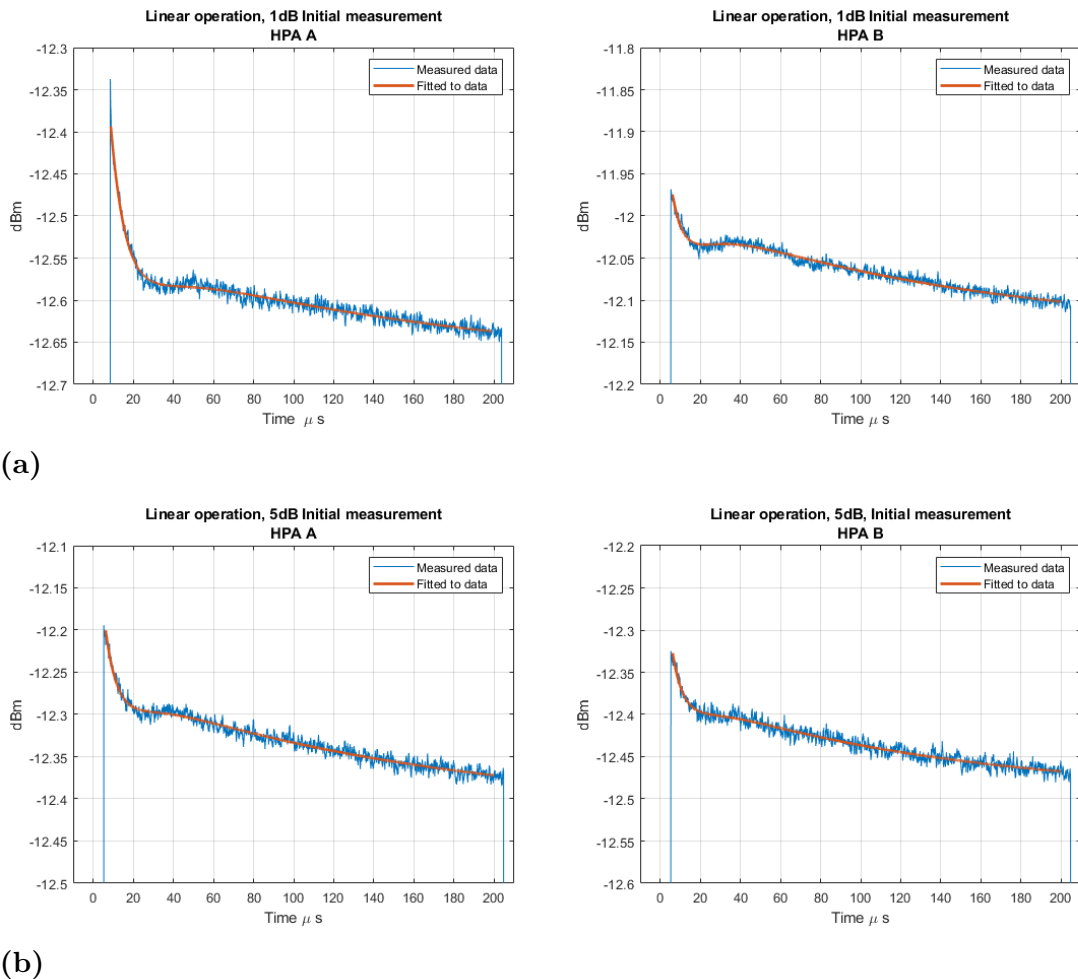


Figure 6.4: Linear operation mode for the initial pulses at the switch non linear and linear for three different compression points 1,3 and 5dB for two different version of a HPA. HPA A (left) and HPA B (right).

Table 6.4: The resulting parameters from the model fitting to the measurement data from HPA A for linear operating mode, initial pulses

| Linear operating mode measurement, initial pulses | | | | | | |
|---|-------|-----------------|-------|-----------------|-------|-----------------|
| Parameters | C_1 | $\tau_1(\mu s)$ | C_2 | $\tau_2(\mu s)$ | C_3 | $\tau_3(\mu s)$ |
| 1dB | 0.482 | 8.041 | 0.274 | 12.50 | 0.185 | 239.2 |
| 3dB | 0.523 | 7.250 | 0.290 | 10.84 | 0.164 | 173.2 |
| 5dB | 0.638 | 7.457 | 0.385 | 10.42 | 0.155 | 155.5 |

Table 6.5: The resulting parameters from the model fitting to the measurement data from HPA B for linear operating mode, initial pulses.

| Linear operating mode measurement, initial pulses | | | | | | |
|---|-------|-----------------|-------|-----------------|-------|-----------------|
| Parameters | C_1 | $\tau_1(\mu s)$ | C_2 | $\tau_2(\mu s)$ | C_3 | $\tau_3(\mu s)$ |
| 1dB | 0.445 | 6.662 | 0.261 | 11.16 | 0.146 | 147.9 |
| 3dB | 0.471 | 9.734 | 0.306 | 13.02 | 0.136 | 215.8 |
| 5dB | 0.514 | 6.891 | 0.355 | 9.167 | 0.125 | 131.6 |

Since the linear operating mode reference measurements have the same input power for all measurements and are expected to be in steady state the results could be expected to be similar. This is also the case as linear operating mode reference measurement as illustrated in figure 6.5 appears with power levels similar to each other. Thus it does not appear to be any power level offset between the compression point measurements for the respective amplifier for the linear reference measurement. The previous measurement for initial pulses in the linear operation mode seen in figure 6.4 however displayed an offset in power level. However, there is one minor difference between HPA A and B which is the reduced second transient for HPA B.

The fitted model parameters for the linear operating mode reference measurements seen in figure 6.6 for HPA A and figure 6.7 for HPA B also indicate that for reference measurements, the fitted coefficients are reduced compared to the previously fitted parameters for initial pulses for the linear operating mode. Thus for the linear operating reference measurement the C_1 parameter has been reduced by a factor of 2 and the C_2 parameter has also seen a similar decrease in comparison to corresponding model parameters in table 6.4 and table 6.5. However, the C_3 parameter remains quite similar to the initial measurements for the linear case. Furthermore, the parameters also indicate that for the linear reference measurements the fitted parameters in table 6.6 and table 6.7 are quite similar for the two amplifiers. For example in the previous measurement of initial pulses for linear operating mode there was an increase in C_1 and C_2 due to previous input drive power levels as seen in table 6.4 and table 6.5. However, in the case of the linear reference measurement, this increase due to previous input is not discernible any longer as seen in table 6.6 and table 6.7. This would be consistent with a memory effect that is present for the initial pulses but as the amplifiers achieve steady state the effects are no longer present. Note however that the HPA B sees a dramatic decrease in C_2 which coincides with the observed smaller second transient even though the fitted parameter indicates a much larger decrease than visually indicated.

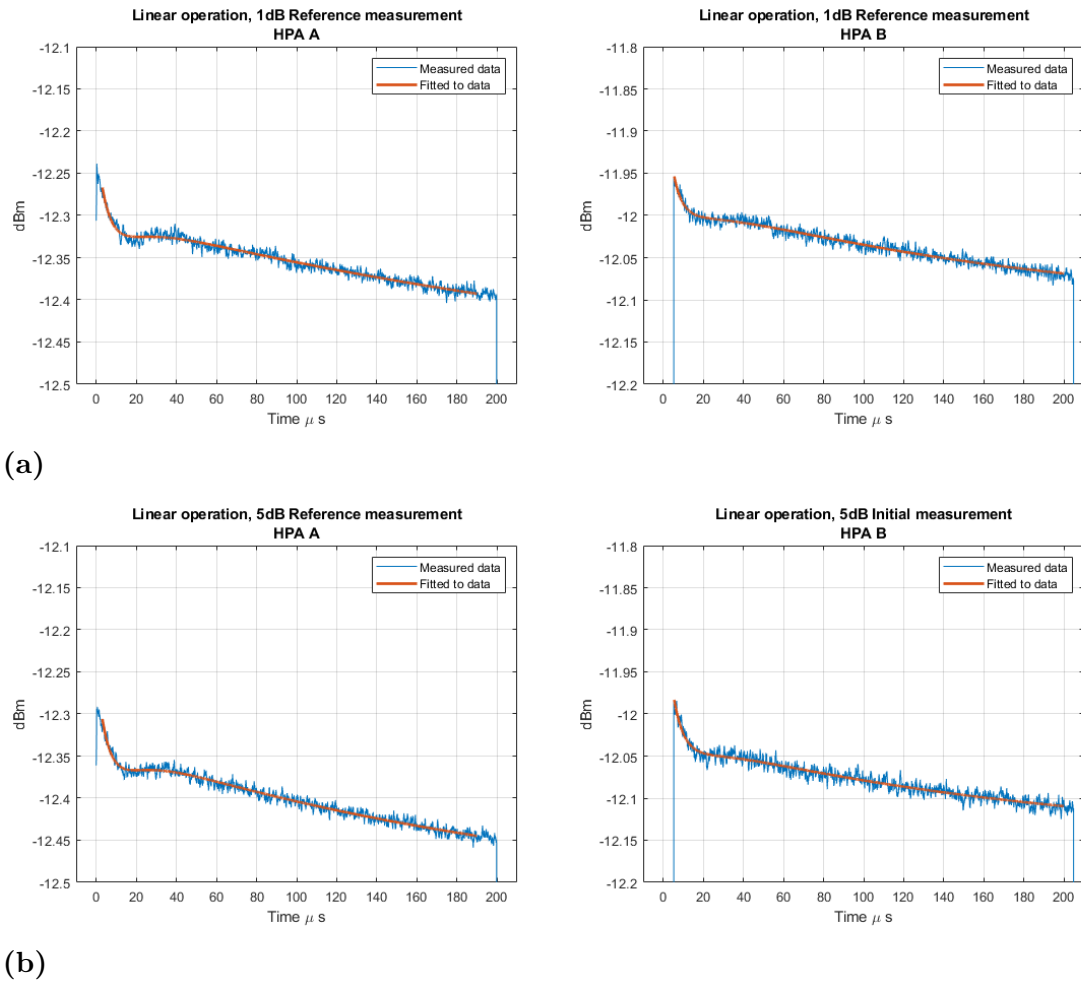


Figure 6.5: Linear operation mode reference measurement 10 min after switch for two different compression points 1 and 5dB for HPA A and B.

Table 6.6: The resulting parameters from the model fitting to the measurement data from HPA A for linear operating mode, reference measurement.

| Linear operating mode measurement, reference measurement | | | | | | |
|--|-------|-----------------|-------|-----------------|-------|-----------------|
| Parameters | C_1 | $\tau_1(\mu s)$ | C_2 | $\tau_2(\mu s)$ | C_3 | $\tau_3(\mu s)$ |
| 1dB | 0.276 | 6.495 | 0.185 | 10.01 | 0.214 | 338.7 |
| 3dB | 0.293 | 7.023 | 0.223 | 11.75 | 0.175 | 182.1 |
| 5dB | 0.264 | 6.132 | 0.172 | 10.59 | 0.172 | 226.0 |

Table 6.7: The resulting parameters from the model fitting to the measurement data from HPA B for linear operating mode, reference measurement.

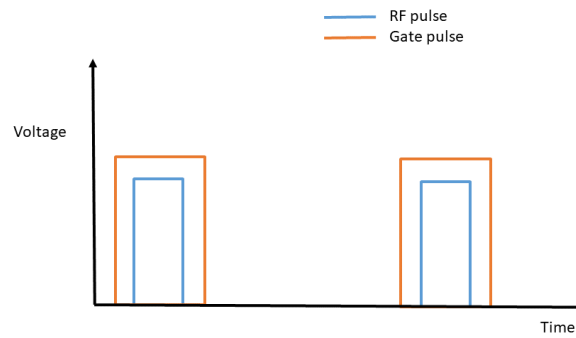
| Linear operating mode measurement, reference measurement | | | | | | |
|--|-------|-----------------|-------|-----------------|-------|-----------------|
| Parameters | C_1 | $\tau_1(\mu s)$ | C_2 | $\tau_2(\mu s)$ | C_3 | $\tau_3(\mu s)$ |
| 1dB | 0.183 | 4.437 | 0.037 | 24.8 | 0.141 | 172.3 |
| 3dB | 0.234 | 3.629 | 0.022 | 26.2 | 0.125 | 147.4 |
| 5dB | 0.305 | 2.713 | 0.003 | 19.4 | 0.082 | 159.7 |

6.2 Test case 2

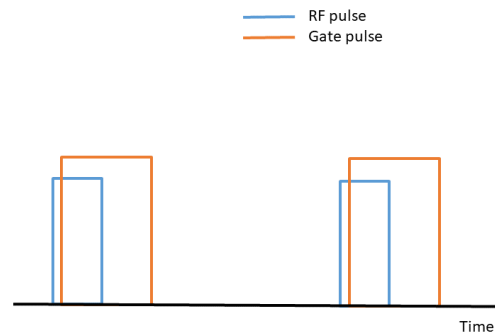
This measurement case is indented to investigate the effects on memory effects and HPA performance by introducing a delay between the gate and RF pulse which is of relevance for system design in terms of timing. The measurement procedure itself is identical to the one performed while investigating the impact of switching from compression to a lower amplitude waveform and settings are displayed in table 6.8. The main difference between the previous measurement case is illustrated in figure 6.6 that instead of applying a gate pulse $2.5\mu s$ before the RF pulse the gate pulse is delayed to $2\mu s$ after RF pulse is applied at the amplifier input.

Table 6.8: Settings used to investigate the impact of gate and RF pulsing time mismatch.

| Operation mode | PRI (ms) | Duty cycle (%) |
|----------------|----------|----------------|
| Non linear | 2 | 10 |
| Linear | 2 | 10 |



(a)

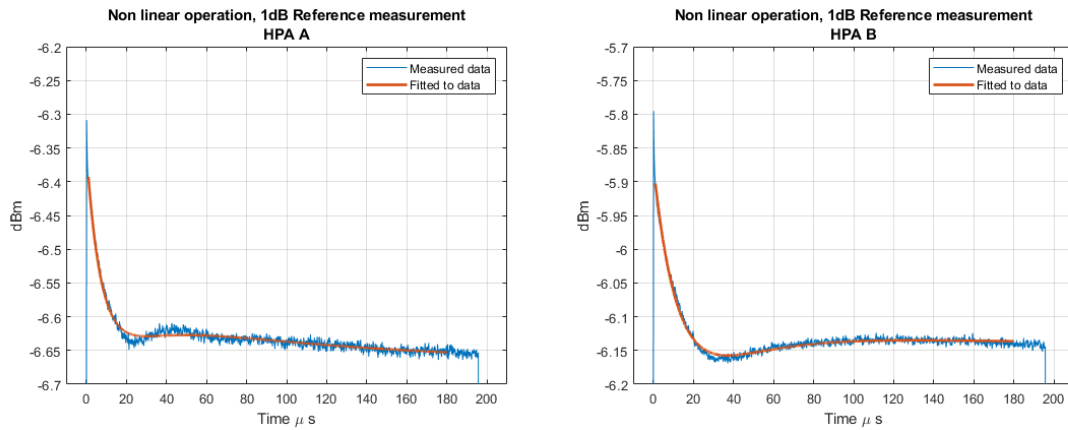


(b)

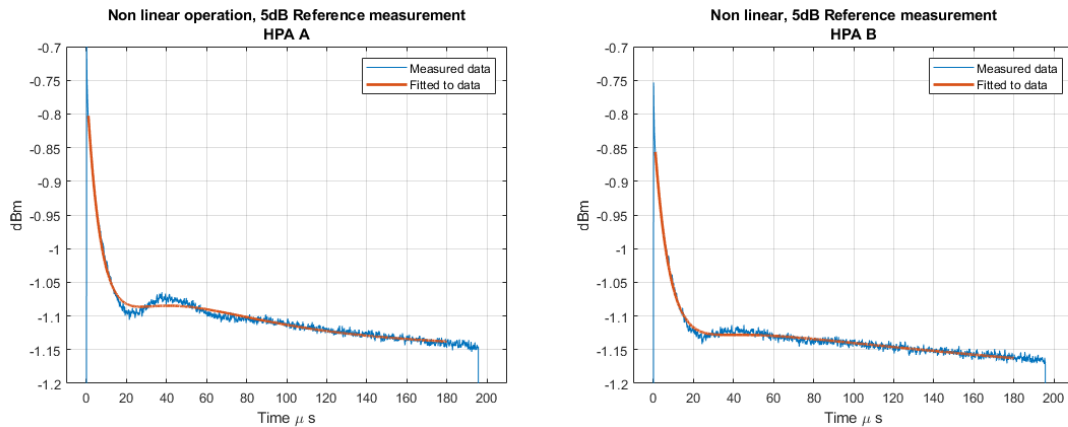
Figure 6.6: The gate and RF pulse mismatch, note that RF pulse is applied before gate pulse, note that illustration is not to scale.

The non linear mode reference measurements seen in figure 6.7 show that the initial transient has a significantly larger impact compared to the corresponding measurement in test case 1 where RF pulses were applied after gate pulse. The second and third transient does not visually appear to differ. However, comparing the HPA A and B show that there are some differences, for example the HPA B, 1dB compression does not, however, appear to have a noticeable third transient.

The fitted model parameters for the non linear reference measurement in table 6.11 for HPA A and 6.12 for HPA B indicate that the initial transient has the highest amplitude and fastest time constant. However, the difference between them is more significant as especially the C_1 parameter is much larger compare to the other constants. Furthermore, a similar trend with increasing C_1 and C_2 constants with increased input drive power level is present. The HPA B indicates slightly higher values than HPA A but the two amplifiers perform similarly in terms of fitted parameters.



(a)



(b)

Figure 6.7: Non linear operation mode measurement for two compression points 1 and 5dB for HPA A (left) and HPA B (right).

Table 6.9: The resulting parameters are from the model fitting to the non linear high power operation mode reference measurement for HPA A, mismatched pulsing, for three compression points.

| Non linear operation reference measurement HPA A | | | | | | |
|--|-------|-----------------|-------|-----------------|-------|-----------------|
| Parameters | C_1 | $\tau_1(\mu s)$ | C_2 | $\tau_2(\mu s)$ | C_3 | $\tau_3(\mu s)$ |
| 1dB | 0.365 | 7.51 | 0.135 | 21.18 | 0.086 | 94.21 |
| 3dB | 0.414 | 7.30 | 0.153 | 20.28 | 0.090 | 89.04 |
| 5dB | 0.555 | 7.52 | 0.250 | 13.10 | 0.198 | 291.07 |

Table 6.10: The resulting parameters are from the model fitting to the non linear high power operation mode reference measurement for HPA B, mismatched pulsing, for three compression points.

| Non linear operation reference measurement HPA B | | | | | | |
|--|-------|-----------------|-------|-----------------|-------|-----------------|
| Parameters | C_1 | $\tau_1(\mu s)$ | C_2 | $\tau_2(\mu s)$ | C_3 | $\tau_3(\mu s)$ |
| 1dB | 0.503 | 13.04 | 0.256 | 25.9 | 0.025 | 225.3 |
| 3dB | 0.846 | 8.46 | 0.182 | 19.4 | 0.086 | 94.5 |
| 5dB | 0.872 | 8.72 | 0.234 | 14.3 | 0.162 | 390.3 |

The initial measurement of linear operating mode in figure 6.8 also indicate the same behaviour as seen in the reference measurement for the non linear with more significant C_1 and C_2 . The fitted model parameters in in table 6.11 and table 6.12 for HPA B and A also indicate an increase in C_1 and C_2 compared to corresponding measurement in test case 1, table 6.4 and table 6.5. Furthermore the model parameters in the mismatched gate and RF pulse also shows a similar increase of transient C_1 and C_2 with increased input drive power levels as previously seen.

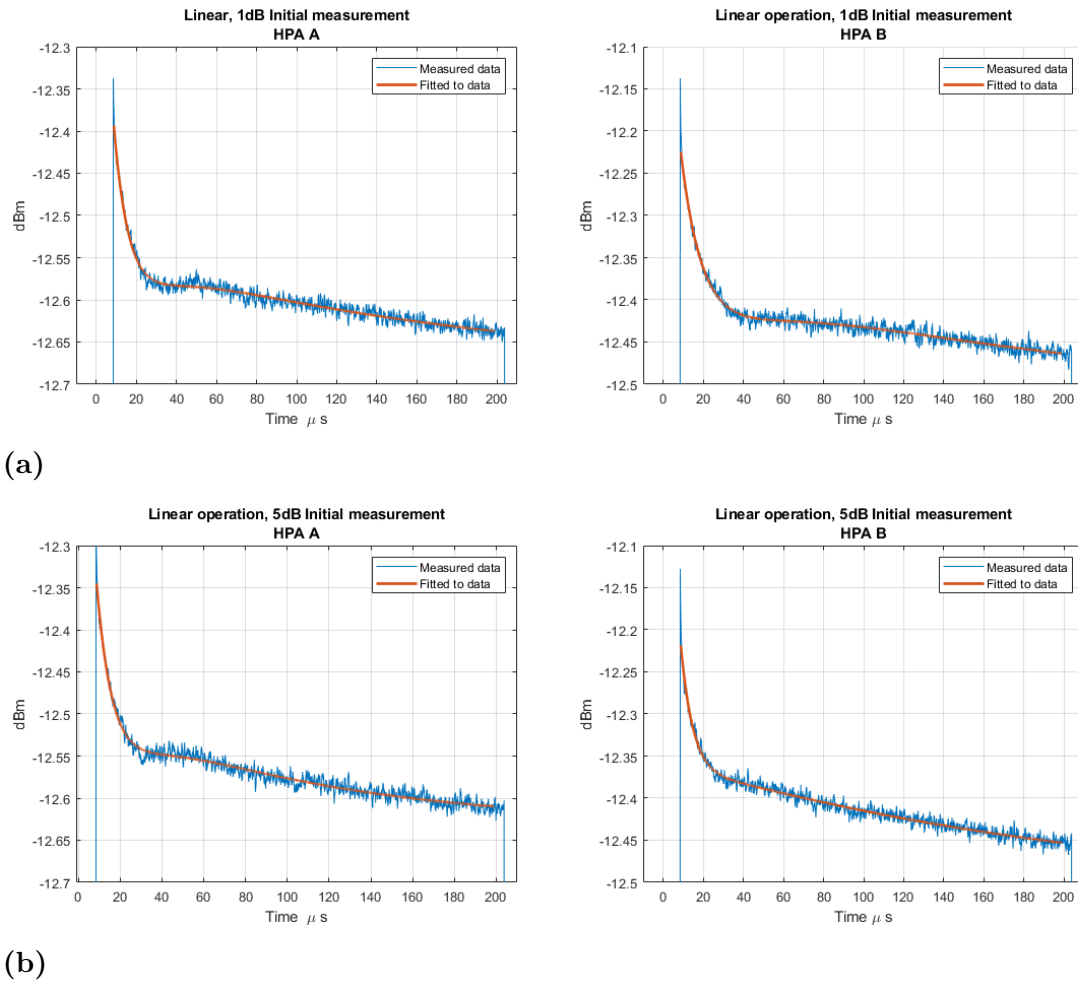


Figure 6.8: Linear operation mode initial measurement , HPA A (left) and HPA B (right).

Table 6.11: The resulting parameters from the model fitting to the measurement data from HPA A for linear operating mode, initial pulses for mismatched pulsing.

| Linear operating mode measurement initial pulses HPA A | | | | | | |
|--|-------|-----------------|-------|-----------------|-------|-----------------|
| Parameters | C_1 | $\tau_1(\mu s)$ | C_2 | $\tau_2(\mu s)$ | C_3 | $\tau_3(\mu s)$ |
| 1dB | 0.926 | 8.52 | 0.317 | 14.9 | 0.142 | 177.5 |
| 3dB | 0.910 | 8.60 | 0.336 | 15.3 | 0.143 | 110.2 |
| 5dB | 0.995 | 8.58 | 0.369 | 14.9 | 0.145 | 102.8 |

Table 6.12: The resulting parameters from the model fitting to the measurement data from HPA A for linear operating mode, initial pulses for mismatched pulsing.

| Linear operating mode measurement initial pulses HPA B | | | | | | |
|--|-------|-----------------|-------|-----------------|-------|-----------------|
| Parameters | C_1 | $\tau_1(\mu s)$ | C_2 | $\tau_2(\mu s)$ | C_3 | $\tau_3(\mu s)$ |
| 1dB | 0.523 | 10.8 | 0.197 | 51.22 | 0.225 | 120.2 |
| 3dB | 0.855 | 5.286 | 0.238 | 64.05 | 0.355 | 90.55 |
| 5dB | 0.892 | 6.84 | 0.279 | 8.900 | 0.166 | 220.3 |

The linear operating mode reference measurement for the mismatched gate pulse case visible shows a stronger impact of the first and second transient. This is seen when compared to the corresponding linear operating mode reference measurement in the previous case. Furthermore, the parameters in table 6.13 and table 6.14 for HPA A and B which both shows a sharp decline in amplitude compared to the initial linear operating mode measurement and the values for the initial transient as seen in table 6.11 and table 6.12 for HPA A and B. The decrease of the C_2 parameter shows only a small amount of decrease. Especially compared to the corresponding linear operating mode measurement in the previous case where the decrease in C_2 was significant. However, the third transient shows no significant change for either of the amplifiers.

Table 6.13: The resulting parameters from the model fitting to the measurement data from HPA A for linear operating mode, reference measurement, mismatched pulse case.

| Linear operating mode reference measurement HPA A | | | | | | |
|---|-------|-----------------|-------|-----------------|-------|-----------------|
| Parameters | C_1 | $\tau_1(\mu s)$ | C_2 | $\tau_2(\mu s)$ | C_3 | $\tau_3(\mu s)$ |
| 1dB | 0.463 | 9.30 | 0.315 | 13.7 | 0.129 | 140.1 |
| 3dB | 0.445 | 8.95 | 0.315 | 13.9 | 0.140 | 125.0 |
| 5dB | 0.458 | 9.66 | 0.334 | 15.3 | 0.146 | 98.28 |

Table 6.14: The resulting parameters from the model fitting to the measurement data from HPA B for linear operating mode, reference measurement.

| Linear operating mode reference measurement, HPA B | | | | | | |
|--|-------|-----------------|-------|-----------------|-------|-----------------|
| Parameters | C_1 | $\tau_1(\mu s)$ | C_2 | $\tau_2(\mu s)$ | C_3 | $\tau_3(\mu s)$ |
| 1dB | 0.205 | 10.31 | 0.155 | 43.39 | 0.194 | 99.21 |
| 3dB | 0.339 | 8.522 | 0.236 | 12.01 | 0.150 | 140.4 |
| 5dB | 0.337 | 6.787 | 0.217 | 9.025 | 0.153 | 160.6 |

6. Measurement results

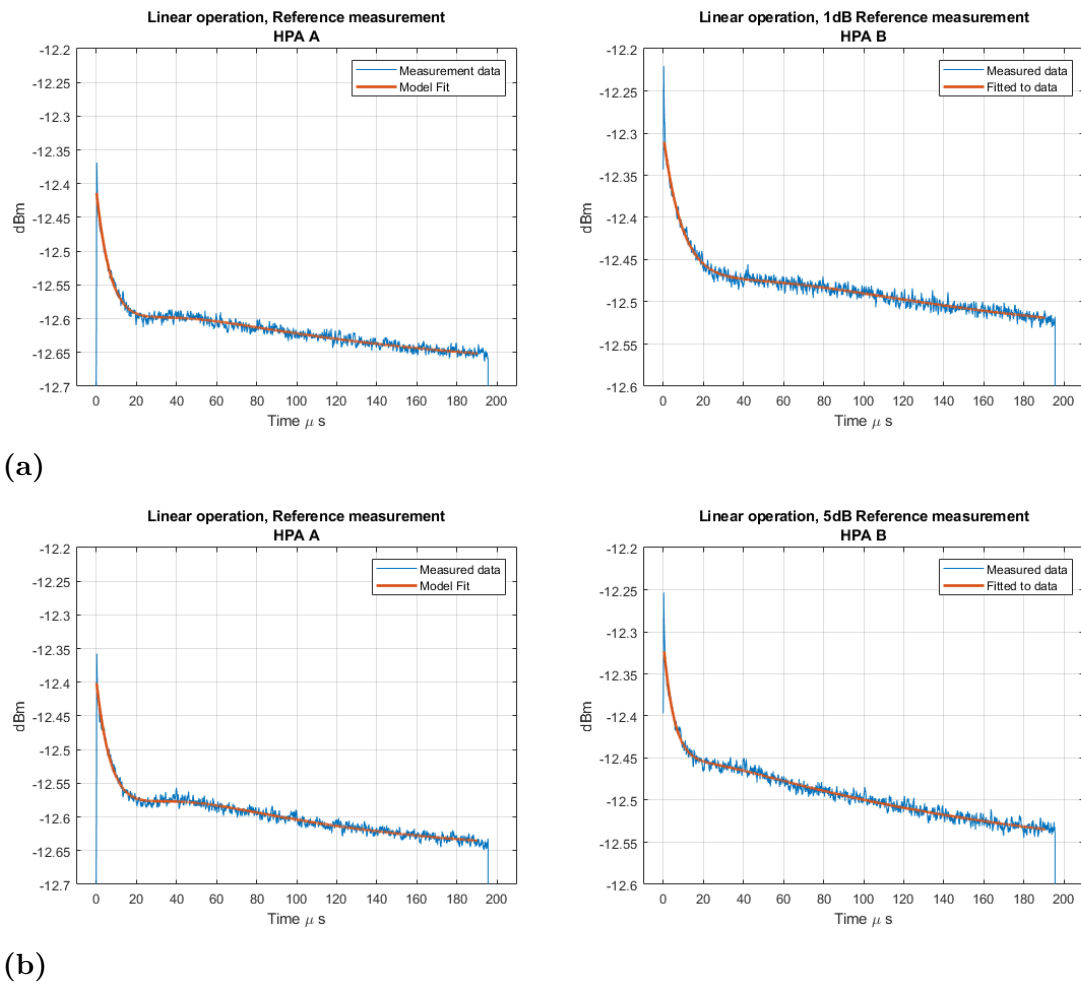


Figure 6.9: Linear operation mode reference measurement, 10 min after switch from non linear , HPA A (left) and HPA B (right).

6.3 Test case 3

The third test case involves switching from pulsed operation in non linear regime, to a long waveform with a lower drive input power in the linear regime of the amplifiers. In terms of multi function sensors, this could be relevant when for example switching from radar to a communication system. Unlike the previous measurement scenario, the continuous wave starts the moment the last pulse in the non linear operating mode ends with the linear operating mode starting immediately as seen in figure 6.10. For the linear operating condition a 6 ms long pulse in order to enable the investigation of long term recovery of the HPA. There have been previous studies indicating a longer recovery time after stressing a device with a significant high power pulse driving the device in deep compression [14]. This test however is focused on slightly lower input power levels such as the 1dB to 5dB compression points, linear operating mode. The most significant difference is that the HPA is operating in non linear mode for a longer time, achieving steady state before switching to linear operating mode.

Furthermore, this measurement takes the behavior of the amplifiers over 6.2 ms into account and will also include the measured current to provide additional information on the performance over this time. For the pulse, the same settings are detailed in 6.15 and for the nonlinear power levels corresponding to 1dB, 3dB and 5dB compression with the gate pulsing being applied before RF. Therefore the waveform 1 is identical to that of the measurement case with the gate pulse applied before RF.

Table 6.15: Settings used in the pulsed to continuous wave measurement.

| Operation mode | PRI (ms) | Duty cycle (%) |
|----------------|----------|----------------|
| Non linear | 2 | 10 |
| Linear | 6 | 100 |

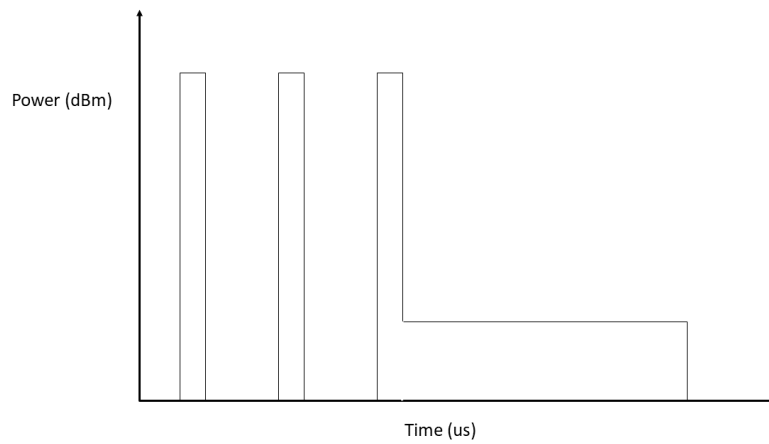


Figure 6.10: Illustration of measurement scenario, not to scale. The non linear operating mode is pulsed and high power and is switched to linear operating mode and a long pulse illustrated by a 6ms trailing RF modulated pulse.

From figure 6.11 containing the measurements results for the three cases of HPA with different drive input power levels and then switching to a CW case. For the previous amplifier version to the left, the main discernable differences are that it appears that for the higher input power the result is a deeper dip in amplification and then an upward trend, increase in gain. The 3dB and 5dB measurements show that in both cases converge after time with each other while the 1dB compression point is subject to an offset for both versions of the amplifier. However, as the measurements are performed in succession with a cool down period so a small change between the results for the different compression point measurements could be possible such as the case of HPA B. Thus the significant offset seen for HPA A is surprising and it has also been possible to replicate this behavior at separate occasions. Furthermore, for both the 5dB measurements for the amplifiers there is a noticeable dip in gain directly at the switch between non linear operating mode and linear. This is more clearly seen in the magnified graphs in the lower part of figure 6.11. For the 3dB case, a very slight dip is also present but not as significant.

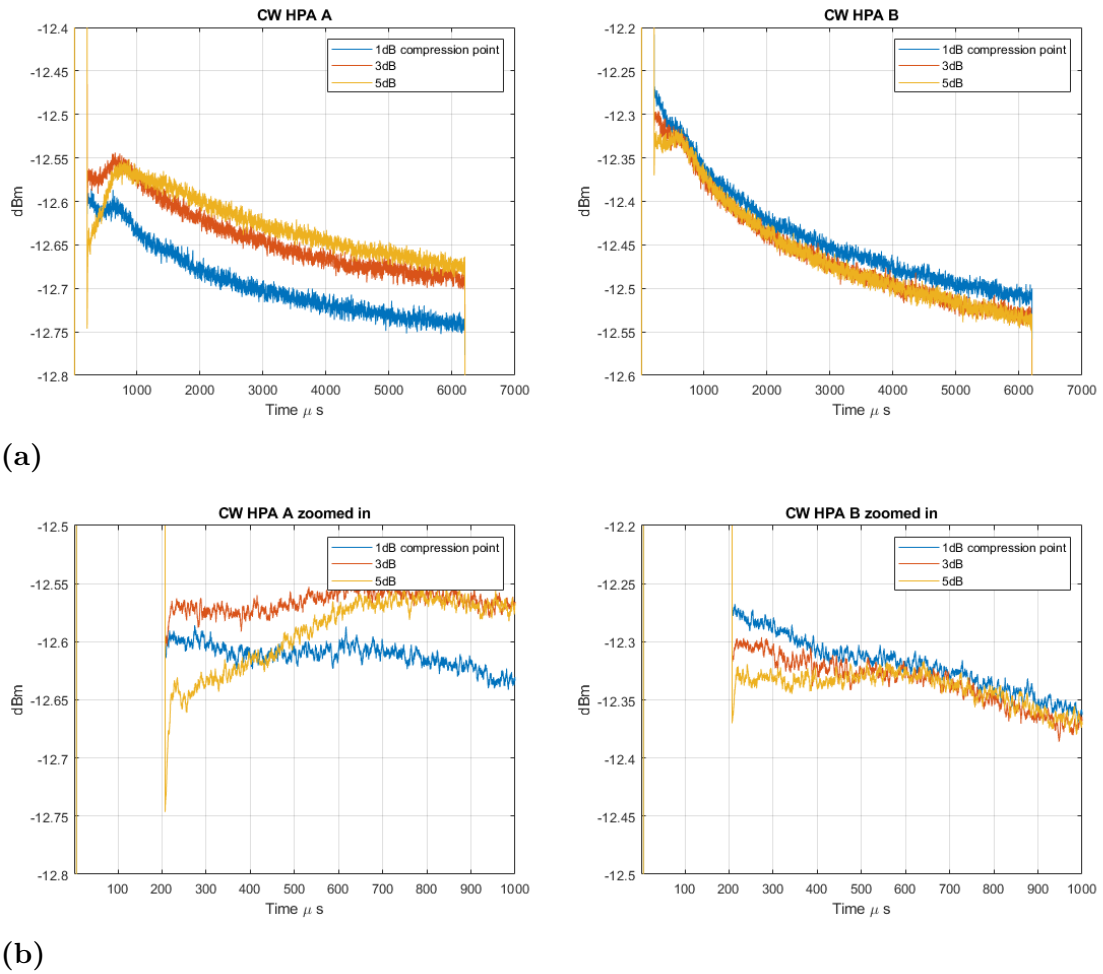
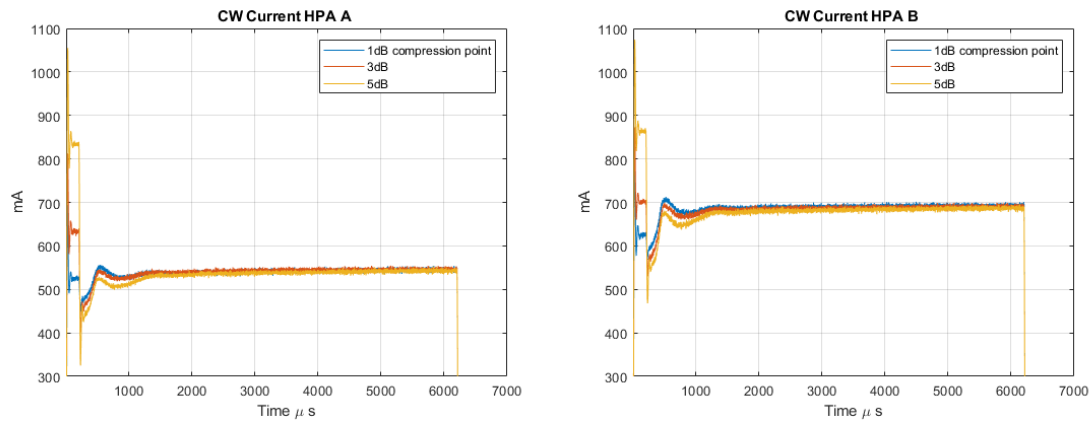
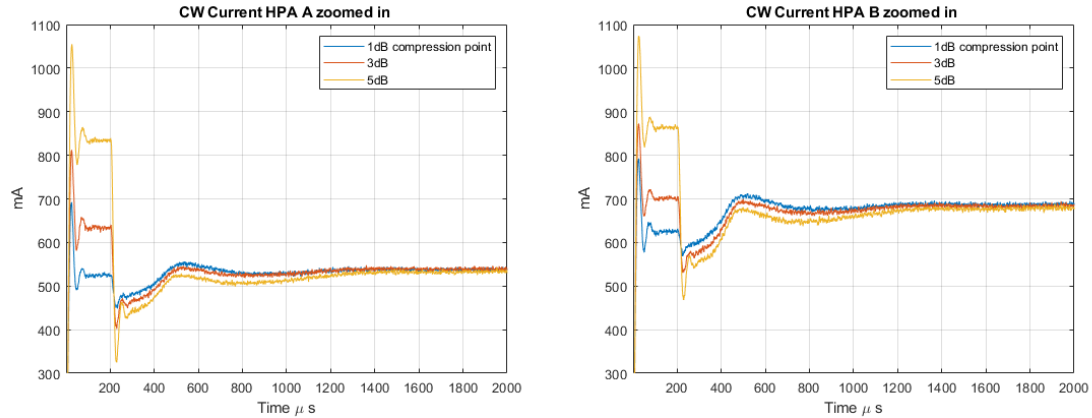


Figure 6.11: The measured switch between pulsed RF and CW with the measurement starting with the last pulse and then CW for two versions of an amplifier. The more recent version to the right and the older version to the left. The bottom half provides a zoomed in version to the above measurements.

The current measurement as seen in figure 6.12 shows a decrease of current during switching followed by an increase to up until the time $700 \mu s$ when an oscillating motion occurs as the current consumption start to converge at about $1200 \mu s$. During this period it appears that the 1dB case requires more current compared to 3 and 5dB. Furthermore, the figure differs slightly in that the more recent amplifier consumes more current but otherwise rather similar. Unlike the case regarding power. Note that the power in HPA A and B for the initial 1 ms shows different characteristics especially in regard to that the current does not seem to differ significantly. There are some differences such as the amount of current during the CW.



(a)



(b)

Figure 6.12: The measured current during switch from pulsed to CW. Note that the below graphs are zoomed in around the waveform switch.

7

Conclusion

To enable characterization of memory effects in the intended HPAs required the designing and implementation of a sufficiently advanced test bench able to perform the change in applications and perform the measurement. The resulting test bench has proven useful for characterizing transients in HPAs and switching between different operation modes with waveform sequencing also proved successful.

The measurements conducted and presented included investigation of the impact of switching from a high amplitude waveform being operated in non linear and switching to linear operating mode. By comparing the measurement of the initial pulses of linear operation with the reference measurement for non linear and linear operation indicates an increase in the amplitude of the first and second transients as the input power in non linear mode. As time progressed the reference measurement for the linear operation did not show the same dependence, thus the effect from the previous waveform was noticeable only for the initial pulses, which is consistent with memory effects. This was also seen in the model for the C_2 and C_1 parameters. The third transient did not appear affected by the previous input which implies that the main effects of memory effects, in this case, are most significant during the first part of the pulse which was indicated in both devices.

By performing the same experiment but changing the timing of the gate pulsing to occur not before but after the RF pulse to investigate the effect of timing and other effects present at the enabling of the device. Similar behavior with increased transient one and two in terms of amplitude due to increased input drive power. However, the first and second transient was more significant also at thermal equilibrium for the linear reference measurement. This was the case for both HPA A and B and this indicates a more significant presence of these two transient overall in the case of changing the timing between gate and RF pulses. Thus illustrating the need to consider the timing as applying the RF pulse after the gate pulse had a significant effect.

The third case investigating the scenario of switching from pulsed to continuous wave indicated a 1-2 ms process for the 3 and 5dB compression point to converge to similar values while 1dB did not converge during the investigated time span of 6ms. The current measurement for the continuous waveform also indicated a potential discrepancy in that the current in HPA A did not align with the output as the HPA B. However this indicates that the recovery time and presence of memory effects also in the CW case increase with increased power in the previous non linear operating mode. Furthermore that the effects are prominent during several microseconds which is important to be aware of if the amplifier is intended to be used for applications requiring a time invariant gain.

The results of this thesis provide insights into the impact of memory effects on these two amplifier versions which are not only useful for understanding the operation of the device in order to improve upon a design or make changes in fabrication. The presented information is also useful for the system designers that work with AESA multi function sensors. In this respect, the thesis has provided insight and contributed to the process of further develop GaN MMIC based HPAs for use in multi function sensor systems by characterizing memory effects.

8

Future work

The work presented in this thesis could be expanded to include more measurements on several amplifiers of the same model and version to acquire statistics about the effect of memory effects on the average HPA. Both to verify the models but also to investigate the potential spread and variation of these effects over several devices. This could also be extended to include characterization of other models of amplifiers than the particular one used during this thesis. Furthermore, since the memory effects in this thesis were studied in terms of initial pulses of the linear operating mode being compared with two reference measurements but it would also be of interest to further study the initial pulses in order to determine if there are significant changes between the different initial pulses. For example how the first pulse in the linear case compares with the second, third, or tenth pulse after the switch from non linear operating mode.

Due to the significant impact caused by the timing mismatch between gate and RF pulses, it would be of interest to conduct a more rigorous investigation into the effects of the gate and RF mismatch. Especially to determine if the impact on transients are further lessened the longer the gate is enabled or if the impact of these transient are decreased when the gate is enabled a few ns before RF is applied. It could also be of interest to perform these measurements on the device on a thermal chuck in order to test the device in a more thermally controlled environment to investigate the effect of temperature on memory effect. This could also be combined with attempting to develop methods for determining the temperature of the HPAs.

9

Environmental and ethical aspects

The use of multi function sensor systems with GaN MMIC technology has the potential to reduce power consumption as well as decrease the amount of hardware required if one system can perform several tasks. This could potentially have a positive environmental impact in terms of reducing the required resources to realize these systems. All technology, multi function sensors not being an exception can potentially be used for military applications, especially since Saab is a company active within the defense industry. This does not however pose an inherent ethical dilemma but engineers active in this field should be aware of this.

Bibliography

- [1] P. W. Moo and D. J. DiFilippo, “Overview of naval multifunction rf systems,” in *2018 15th European Radar Conference (EuRAD)*, pp. 178–181, 2018.
- [2] H. van Bezouwen, H. Feldle, and W. Holpp, “Status and trends in aesa-based radar,” pp. 526–529, 2010.
- [3] N. Billström, J. Nilsson, A. Tengs, and N. Rorsman, “High performance gan front-end mmics,” in *2011 6th European Microwave Integrated Circuit Conference*, pp. 348–351, 2011.
- [4] D. Ueda, *Properties and Advantages of Gallium Nitride*, pp. 1–26. Cham: Springer International Publishing, 2017.
- [5] O. Axelsson, S. Gustafsson, H. Hjelmgren, N. Rorsman, H. Blanck, J. Splettstoesser, J. Thorpe, T. Roedle, and M. Thorsell, “Application relevant evaluation of trapping effects in algan/gan hemts with fe-doped buffer,” *IEEE Transactions on Electron Devices*, vol. 63, no. 1, pp. 326–332, 2016.
- [6] P. M. Tome, F. M. Barradas, T. R. Cunha, and J. C. Pedro, “Compensation of the pulse-to-pulse instability of gan hemt-based power amplifiers,” in *2019 IEEE MTT-S International Microwave Symposium (IMS)*, pp. 408–411, 2019.
- [7] C. G. Tua, T. Pratt, and A. I. Zaghloul, “A study of interpulse instability in gallium nitride power amplifiers in multifunction radars,” *IEEE Transactions on Microwave Theory and Techniques*, vol. 64, no. 11, pp. 3732–3747, 2016.
- [8] J. Bergsten, M. Thorsell, D. Adolph, J. Chen, O. Kordina, E. Sveinbjörnsson, and N. Rorsman, “Electron Trapping in Extended Defects in Microwave Al-GaN/GaN HEMTs With Carbon-Doped Buffers,” *IEEE Transactions on Electron Devices*, vol. 65, no. 6, pp. 2446–2453, 2018.
- [9] L. Hanning, “Pulse shaping of radar transmitters: Compensation of memory effects through digital pre-distortion,” Master’s thesis, Department of Electrical Engineering, Chalmers University of Technology, 2018.
- [10] H. van Bezouwen, H. Feldle, and W. Holpp, “Status and trends in aesa-based radar,” in *2010 IEEE MTT-S International Microwave Symposium*, pp. 526–529, 2010.
- [11] S. J. A. H. W. A. Richards, Mark A., *Principles of Modern Radar, Volume I - Basic Principles*. SciTech Publishing, 2010.
- [12] U. K. Mishra, L. Shen, T. E. Kazior, and Y. Wu, “Gan-based rf power devices and amplifiers,” *Proceedings of the IEEE*, vol. 96, no. 2, pp. 287–305, 2008.
- [13] M. Rais-Zadeh, V. J. Gokhale, A. Ansari, M. Faucher, D. Théron, Y. Cordier, and L. Buchaillot, “Gallium nitride as an electromechanical material,” *Journal of Microelectromechanical Systems*, vol. 23, no. 6, pp. 1252–1271, 2014.

- [14] O. Axelsson, N. Billström, N. Rorsman, and M. Thorsell, “Impact of trapping effects on the recovery time of gan based low noise amplifiers,” *IEEE Microwave and Wireless Components Letters*, vol. 26, no. 1, pp. 31–33, 2016.
- [15] J. Bergsten, *Buffer Related Dispersive Effects in Microwave GaN HEMTs*. PhD thesis, Department of Microtechnology and Nanoscience, Chalmers University of Technology, 2018.
- [16] M. Sudow, M. Fagerlind, M. Thorsell, K. Andersson, N. Billstrom, P. Nilsson, and N. Rorsman, “An AlGaIn/GaN HEMT-Based microstrip MMIC Process for Advanced Transceiver Design,” *IEEE Transactions on Microwave Theory and Techniques*, vol. 56, no. 8, pp. 1827–1833, 2008.
- [17] Keysight Technologies, “Keysight M8190A arbitrary waveform generator, user’s guide,” 2017.
- [18] B&Z Technologies, “Bzr-1022-1,” 2014.
- [19] S. Sze and K. Ng, *Physics of semiconductor devices*. Wiley-Interscience, 2007.
- [20] Rhode&Schwarz, “R&S RTO Digital Oscilloscope user manual.”